

# Global Biogeochemical Cycles®



## RESEARCH ARTICLE

10.1029/2024GB008287

## Glacial-Interglacial and Millennial-Scale Changes in Nitrous Oxide Emissions Pathways and Source Regions

### Key Points:

- The isotopic composition of atmospheric N<sub>2</sub>O was determined for the last deglaciation and an abrupt warming event during the last ice age
- The new isotope data allow reconstruction of the emissions of N<sub>2</sub>O to the atmosphere from microbial nitrification versus denitrification
- The source reconstructions highlight the sensitivity of N<sub>2</sub>O emissions to climate warming in both marine and terrestrial environments

J. A. Menking<sup>1,2,3</sup> , J. E. Lee<sup>1,4</sup> , E. J. Brook<sup>1</sup>, J. Schmitt<sup>5</sup> , L. Soussaintjean<sup>5</sup>, H. Fischer<sup>5</sup>, J. Kaiser<sup>6</sup> , and A. Rice<sup>7</sup>

<sup>1</sup>College of Earth, Ocean, and Atmospheric Sciences, Oregon State University, Corvallis, OR, USA, <sup>2</sup>Australian Antarctic Program Partnership, Institute for Marine and Antarctic Studies, University of Tasmania, Hobart, TAS, Australia, <sup>3</sup>Environment Research Unit, Commonwealth Scientific and Industrial Research Organisation, Aspendale, VIC, Australia, <sup>4</sup>Los Alamos National Laboratory, Los Alamos, NM, USA, <sup>5</sup>Climate and Environmental Physics, Physics Institute & Oeschger Centre for Climate Change Research, University of Bern, Bern, Switzerland, <sup>6</sup>Centre for Ocean and Atmospheric Sciences, School of Environmental Sciences, University of East Anglia, Norwich, UK, <sup>7</sup>Department of Physics, Portland State University, Portland, OR, USA

### Supporting Information:

Supporting Information may be found in the online version of this article.

### Correspondence to:

J. A. Menking,  
james.menking@utas.edu.au

### Citation:

Menking, J. A., Lee, J. E., Brook, E. J., Schmitt, J., Soussaintjean, L., Fischer, H., et al. (2025). Glacial-interglacial and millennial-scale changes in nitrous oxide emissions pathways and source regions. *Global Biogeochemical Cycles*, 39, e2024GB008287. <https://doi.org/10.1029/2024GB008287>

Received 2 JUL 2024

Accepted 3 APR 2025

### Author Contributions:

**Conceptualization:** J. A. Menking,

E. J. Brook

**Data curation:** J. A. Menking, J. E. Lee, J. Schmitt, H. Fischer

**Formal analysis:** J. A. Menking, J. E. Lee, J. Schmitt, J. Kaiser

**Funding acquisition:** J. A. Menking,

E. J. Brook

**Investigation:** J. A. Menking, J. E. Lee

**Methodology:** J. A. Menking, J. E. Lee,

J. Schmitt, L. Soussaintjean, H. Fischer,

J. Kaiser, A. Rice

**Software:** J. A. Menking

**Validation:** J. A. Menking, H. Fischer,

A. Rice

**Writing – original draft:** J. A. Menking

**Abstract** During the transition from the Last Glacial Maximum (LGM) to the Holocene, the atmospheric N<sub>2</sub>O mole fraction increased by 80 nmol mol<sup>-1</sup>. Using ice core measurements of N<sub>2</sub>O isotopomer ratios, we show that this increase was driven by increases in both nitrification and denitrification, with the relative partitioning between both production pathways depending on the assumed isotopic end-member source signatures. Similarly, we also attribute a 35 nmol mol<sup>-1</sup> N<sub>2</sub>O mole fraction increase during the Heinrich Stadial 4/Dansgaard Oeschger 8 (HS4/DO8) millennial-scale event to increases in both N<sub>2</sub>O production pathways. In contrast, the 25 nmol mol<sup>-1</sup> N<sub>2</sub>O mole fraction decrease during the Younger Dryas was driven almost exclusively by a decrease in nitrification. The deglacial and HS4/DO8 increases in N<sub>2</sub>O production occurred in both marine and terrestrial environments, with the terrestrial source responding faster to warming by about two centuries. Constraints on *changes* in nitrification and denitrification emissions are robust and consistent with previous studies showing the sensitivity of N<sub>2</sub>O emissions to abrupt Northern Hemisphere warming. This study demonstrates for the first time the importance of both denitrification and nitrification pathways in driving source changes. Absolute emissions are more uncertain due to uncertainty about source isotopomer signatures. For instance, the contribution of denitrification to emissions at the LGM shifts from (65 ± 10) % to (91 ± 6) % when factoring in isotope enrichment due to partial reduction of N<sub>2</sub>O to N<sub>2</sub> during denitrification. Reducing uncertainty in source signatures will increase the power of ice core N<sub>2</sub>O isotope records in deducing environmental change.

**Plain Language Summary** Nitrous oxide (N<sub>2</sub>O) is a greenhouse gas that contributes to global warming and stratospheric ozone depletion. Understanding how the amount of N<sub>2</sub>O in the atmosphere will change with climate is important for future predictions, and polar ice cores represent a unique archive to study nitrous oxide variations in the past. Previous ice core N<sub>2</sub>O studies used stable isotope ratios (<sup>15</sup>N/<sup>14</sup>N and <sup>18</sup>O/<sup>16</sup>O in N<sub>2</sub>O) to reconstruct what the change in source flux from marine versus terrestrial environments must have been to cause N<sub>2</sub>O to rise 80 nmol mol<sup>-1</sup> during the last deglaciation, a dramatic global warming that saw the transition from the ice age to interglacial. Here we use intra-molecular isotope ratios (position of <sup>15</sup>N in N<sub>2</sub>O) to reconstruct a plausible change in source flux from nitrification versus denitrification, and we find that both production pathways contributed approximately equally in increasing the atmospheric N<sub>2</sub>O concentration. We reconstruct source changes for a millennial-scale N<sub>2</sub>O variation that occurred about 40,000 years ago and find essentially the same thing—nitrification and denitrification were both important for causing atmospheric N<sub>2</sub>O to change. In the case where the isotope ratio for N<sub>2</sub>O produced from denitrification is higher due to reduction of N<sub>2</sub>O before emission to the atmosphere, denitrification plays a more dominant role in the absolute N<sub>2</sub>O budget, highlighting the importance of future work to address uncertainties in N<sub>2</sub>O source isotopic signatures.

© 2025. The Author(s).

This is an open access article under the terms of the [Creative Commons Attribution License](https://creativecommons.org/licenses/by/4.0/), which permits use,

distribution and reproduction in any medium, provided the original work is properly cited.

## 1. Introduction

Nitrous oxide (N<sub>2</sub>O) is a powerful greenhouse gas and contributes to ozone destruction in the stratosphere (Ciais et al., 2013; Ravishankara et al., 2009). Natural emissions of N<sub>2</sub>O are projected to increase in the future with global warming, but the biogeochemical mechanisms that link climate with N<sub>2</sub>O emissions are not fully

Writing – review & editing:

J. A. Menking, J. E. Lee, E. J. Brook,  
J. Schmitt, L. Soussaintjean, H. Fischer,  
J. Kaiser, A. Rice

understood. Ice cores preserve a record of variations in atmospheric N<sub>2</sub>O mole fractions and isotope signatures, offering a unique way to explore the link between climate and N<sub>2</sub>O production rates and pathways.

N<sub>2</sub>O is a byproduct of microbial nitrification and denitrification in marine and terrestrial ecosystems (Stein & Yung, 2003). Marine sources presently comprise (35 ± 10) % of natural N<sub>2</sub>O emissions (Tian et al., 2020). Dissolved oxygen concentrations, *c*(O<sub>2</sub>), are the primary control on marine emissions (Nevison et al., 2003). Low-*c*(O<sub>2</sub>) regions can have disproportionately large N<sub>2</sub>O production rates via the denitrification pathway (Bange et al., 2001; Dore et al., 1998; Farias et al., 2009; Naqvi et al., 2010), but such regions are estimated to account for only (4.5 ± 1.5) % of total marine emissions due to large gross fluxes associated with N<sub>2</sub>O consumption that reduce net N<sub>2</sub>O production (Battaglia & Joos, 2018). The overwhelming majority of marine N<sub>2</sub>O production (93%–96%) is estimated to result from nitrification (Battaglia & Joos, 2018; Freing et al., 2012; Nevison et al., 2003). Soils comprise (58 ± 10) % of the natural N<sub>2</sub>O emissions source (Butterbach-Bahl et al., 2013; Ciais et al., 2013), primarily through the denitrification pathway (Vilain et al., 2014). The primary controls are soil temperature and moisture content, and availability of organic and inorganic N sources (Bouwman et al., 1993, 2013; Xu et al., 2012). A small fraction of N<sub>2</sub>O ((7 ± 3) %) is produced by lightning, chemical reactions in the atmosphere, and nitrogen cycling in inland and coastal waters (Tian et al., 2020). N<sub>2</sub>O is destroyed in the stratosphere via photolysis and reaction by O(<sup>1</sup>D) with an atmospheric mean lifetime (troposphere and stratosphere) of 123 years (Prather et al., 2015).

Ice core records show glacial-interglacial variations of the atmospheric N<sub>2</sub>O mole fraction up to 80 nmol mol<sup>-1</sup> (Flückiger et al., 1999; Schilt, Baumgartner, Blunier, et al., 2010; Sowers, 2001; Spahni et al., 2005), with variations of 20–60 nmol mol<sup>-1</sup> observed on millennial timescales throughout the last glacial period (Flückiger et al., 1999, 2004; Schilt, Baumgartner, Schwander, et al., 2010; Schilt et al., 2013). Most previous work has suggested that changes in N<sub>2</sub>O source strength in marine and/or terrestrial environments caused the observed atmospheric N<sub>2</sub>O variations rather than changes in the atmospheric lifetime of N<sub>2</sub>O (Flückiger et al., 2004). The similarity of the ice core CO<sub>2</sub> and N<sub>2</sub>O records led researchers to suspect that changes in marine emissions drove past N<sub>2</sub>O fluctuations, with prior work focusing on the role of marine oxygenation in relation to ocean circulation and nutrient delivery (Schmittner & Galbraith, 2008), as well as the activation of marine denitrification “hotspots” (Altabet et al., 2002; Ganeshram et al., 2000; Schmittner et al., 2007). Other studies noted similarity to abrupt CH<sub>4</sub> changes, suggesting that land N<sub>2</sub>O sources were the driver (Schilt, Baumgartner, Blunier, et al., 2010). The latter is supported by the strong feedback between soil moisture and denitrification rates (Bouwman et al., 1993, 2013), and the notion that past climate changes were accompanied by abrupt shifts in tropical rain belts (Rhodes et al., 2015; Wang et al., 2001).

Stable isotopes of nitrogen and oxygen in N<sub>2</sub>O (δ<sup>15</sup>N and δ<sup>18</sup>O) provide a means to understand the drivers of atmospheric variations because the isotopic signatures of N<sub>2</sub>O sources are distinct (Kim & Craig, 1993). Previous work used ice core, firn air, and flask measurements to reconstruct N<sub>2</sub>O isotopic records. Many of these studies focused on the recent atmospheric history and inferred the isotopic signature of the modern anthropogenic source (Prokopiou et al., 2017; Röckmann et al., 2003; Sowers et al., 2002) or characterized temporal trends (Ghosh et al., 2023; Park et al., 2012). A small subset of this work inferred relative N<sub>2</sub>O production in marine versus terrestrial environments based on the observation that N<sub>2</sub>O produced in terrestrial versus marine environments is isotopically distinct (Fischer et al., 2019; Menking et al., 2020; Schilt et al., 2014). The main finding was that the N<sub>2</sub>O isotopic composition did not change substantially across the last deglaciation, implying similar contributions from land and marine sources (Sowers et al., 2003). More detailed records of N<sub>2</sub>O isotopes confirmed this (Fischer et al., 2019; Schilt et al., 2014) and highlighted that terrestrial emissions increased more abruptly at the start of the Bølling-Allerød warming and at the end of the Younger Dryas. Menking et al. (2020) reported N<sub>2</sub>O isotopic variations across a period of glacial inception and decreasing N<sub>2</sub>O mole fraction that occurred 70 ka (where ka signifies thousand years before 1950 CE) and found that both marine and terrestrial emissions declines were important for a decreasing atmospheric N<sub>2</sub>O mole fraction during global cooling. Thus, climate controls N<sub>2</sub>O emissions in both environments for intervals of cooling as well as warming. To date, only one study has published N<sub>2</sub>O isotope data spanning the millennial-scale N<sub>2</sub>O fluctuations of the last ice age. Menking et al. (2020) produced N<sub>2</sub>O isotope records across Dansgaard-Oeschger event 19 (DO19) at 72 ka as well as the onset of DO16/17 at 60 ka. Inverse calculation of the source changes showed roughly equal contributions of marine and terrestrial N<sub>2</sub>O at DO19, but the changes at the onset of DO16/17 were almost exclusively driven by marine emissions (Menking et al., 2020).

Additional information on the average nitrogen isotopic composition ( $\delta^{15}\text{N}_{\text{bulk}}$ ) may be provided by position dependent nitrogen isotope analyses of  $\text{N}_2\text{O}$ , expressed as “site preference” ( $\delta^{15}\text{N}^{\text{SP}}$ ) between the center-position nitrogen ( $\delta^{15}\text{N}_{\alpha}$ ) and terminal-position ( $\delta^{15}\text{N}_{\beta}$ ) isotope deltas:

$$\delta^{15}\text{N}^{\text{SP}} = \delta^{15}\text{N}_{\alpha} - \delta^{15}\text{N}_{\beta} \quad (1)$$

Results from laboratory experiments suggest a significant difference in  $\delta^{15}\text{N}^{\text{SP}}$  for nitrification (+35‰) versus denitrification (0‰) (Sutka et al., 2006). This result appears to be independent of microbial species and substrate isotopic composition. The distinct  $\delta^{15}\text{N}^{\text{SP}}$  for nitrification and denitrification pathways appears to be a common feature of both natural and laboratory settings for an array of microbes in pure cultures (Figures S1 and S2 in Supporting Information S1) (Toyoda et al., 2017). Several authors proposed using  $\delta^{15}\text{N}^{\text{SP}}$  for distinguishing microbial processes of  $\text{N}_2\text{O}$  production (Denk et al., 2017; Popp et al., 2002; Sutka et al., 2003). Others have cautioned against oversimplification of the position-dependent isotopic effects due to complications relating to (a) isotopic fractionation associated with reduction of  $\text{N}_2\text{O}$  that shifts the isotopic composition away from values set upon production (Figure S2 in Supporting Information S1), (b) isotope effects related to type of enzyme used in  $\text{N}_2\text{O}$  production, and (c) potential overlap in source signatures, particularly that of nitrifying microbes and fungal denitrification (see Supporting Information S1) (Lewicka-Szczebak et al., 2014; Ostrom et al., 2007; Park et al., 2011).

Several  $\text{N}_2\text{O}$  isotope studies examined position dependent-isotopes in firm air and ice core samples and observed a positive trend in site preference attributed to increased nitrification due to land use change and increased use of fertilizers in agriculture (Bernard et al., 2006; Park et al., 2012; Prokopiou et al., 2017, 2018; Röckmann et al., 2003). Recently, firm air data from Styx Glacier challenged this conclusion by demonstrating no significant change in  $\text{N}_2\text{O}$  site preference from 1900 to 2021 CE (Ghosh et al., 2023). Only one study has measured position-dependent isotopes of  $\text{N}_2\text{O}$  in ice cores older than the last several centuries (Prokopiou et al., 2018). The data show a  $\delta^{15}\text{N}_{\alpha}$  increase and  $\delta^{15}\text{N}_{\beta}$  decrease during the Little Ice Age (from 1500 to 1700 CE), suggesting enhanced nitrification, but the analytical uncertainties and temporal resolution preclude more detailed interpretation.

Here we use position-dependent  $\text{N}_2\text{O}$  isotope data to test whether the production pathways of  $\text{N}_2\text{O}$  changed during the 80  $\text{nmol mol}^{-1}$  increase at the last deglaciation, adding novel information about  $\text{N}_2\text{O}$  cycling to a period of study where research to date has only been able to deduce relative changes in marine versus terrestrial emissions (Fischer et al., 2019; Schilt et al., 2014; Sowers et al., 2003). To this end, we present a new site preference record derived from ice core samples containing air spanning the deglacial  $\text{N}_2\text{O}$  rise (16.5–13.2 ka). The data extend through the Younger Dryas cooling interval, when  $\text{N}_2\text{O}$  decreased by about 30  $\text{nmol mol}^{-1}$  (13.2–11.9 ka). We also present  $\text{N}_2\text{O}$  isotope records spanning the Heinrich Stadial 4/Dansgaard-Oeschger 8 (HS4/DO8) transition (39.8–35.8 ka), an example of cyclical millennial-scale  $\text{N}_2\text{O}$  variability characteristic of the last ice age. We use the new ice core data to calculate the emissions changes from nitrification versus denitrification needed to explain the isotope and concentration data. We also present new source histories of marine and terrestrial emissions across the HS4/DO8 interval, constrained by  $\delta^{15}\text{N}_{\text{bulk}}$  data from a combination of ice core records. Given the extreme complexity of terrestrial and oceanic  $\text{N}_2\text{O}$  production, our results represent a plausible explanation making use of the most up to date isotopic information about  $\text{N}_2\text{O}$  production pathways. Future work focusing on the attribution of  $\text{N}_2\text{O}$  production to particular process dynamics using isotopes will undoubtedly merit revision.

## 2. Materials and Methods

We present new measurements of  $\text{N}_2\text{O}$  nitrogen and oxygen average stable isotope deltas ( $\delta^{15}\text{N}_{\text{bulk}}$ ,  $\delta^{18}\text{O}$ ) as well as intramolecular nitrogen isotope signatures ( $\delta^{15}\text{N}_{\alpha}$ ,  $\delta^{15}\text{N}_{\beta}$ ,  $\delta^{15}\text{N}^{\text{SP}}$ ) in ice samples from Taylor Glacier (TG) spanning the last deglaciation (22–11 ka) and the HS4/DO8 transition (40–35.8 ka). We also present new measurements of  $\delta^{15}\text{N}_{\text{bulk}}$  and  $\delta^{18}\text{O}$  in ice samples from the WAIS Divide ice core (WDC) and Talos Dome ice core (TALDICE) spanning HS4/DO8 (42–36.5 ka). TG samples were measured at Oregon State University (OSU), while WDC and TALDICE samples were measured at the University of Bern. The two laboratories have used different procedures described separately below.

## 2.1. Taylor Glacier Samples

Ice core samples were retrieved from the ablation zone of TG in the McMurdo Dry Valleys, Antarctica, during the 2014–2015 field season. The air bubbles in TG ice accurately preserve the past atmosphere from discrete intervals, including the penultimate deglaciation (140–120 ka) (Shackleton et al., 2020), the MIS 5–4 transition (74–59 ka) (Menking et al., 2019, 2020, 2022; Shackleton et al., 2021), the last glacial period (46–34 ka) (Bauska et al., 2018), and the last deglaciation (22–11 ka) (Baggenstos et al., 2017, 2018; Bauska et al., 2016; Dyonisius et al., 2020). Due to a unique combination of glacier flow, ice deformation, and surface ablation, old ice is orientated at the surface of TG with isochronous ice layers striking approximately parallel to glacier flow (Aciego et al., 2007; Baggenstos et al., 2017; Kavanaugh & Cuffey, 2009; Kavanaugh et al., 2009). The proximity of old ice to the surface means that larger samples can be collected quickly and inexpensively compared to traditional drilling methods, proving valuable for trace gas isotope studies (Bauska et al., 2016, 2018; Buizert et al., 2014; Dyonisius et al., 2020; Menking et al., 2019, 2020, 2022; Petrenko et al., 2017; Schilt et al., 2014; Shackleton et al., 2020, 2021).

Samples were collected using a hand-operated PICO drill and a custom core-retrieval tool. Sample collection occurred at approximately 1 m intervals along a horizontal transect beginning at a depth of 4 m to avoid thermal cracks that propagate from the surface of the ice (Baggenstos et al., 2017). The age of the gas bubbles for the samples in this study has been well-characterized by previous work relating CH<sub>4</sub> and CO<sub>2</sub> mole fractions to established ice core chronologies (Baggenstos et al., 2018; Buizert, Cuffey, et al., 2015; Schilt et al., 2014).

We extracted air from 60 TG ice samples ranging from 0.8 to 2 kg using a dry “cheese grater” technique at OSU (Bauska et al., 2016; Etheridge et al., 1996) resulting in air samples of estimated size 50–200 cm<sup>3</sup> (20°C, 1 bar). To extract and purify N<sub>2</sub>O, the air was dried in an H<sub>2</sub>O trap at –105°C while CO<sub>2</sub> and N<sub>2</sub>O were trapped at –195°C (Menking et al., 2020; Schilt et al., 2014). The mixture was passed through Ascarite (NaOH-coated silica) for CO<sub>2</sub> removal and Mg(ClO<sub>4</sub>)<sub>2</sub> for further H<sub>2</sub>O removal. The purified N<sub>2</sub>O was preconcentrated twice on successively smaller volumes of stainless steel tubing and fused silica capillary and then passed through a PoraBOND Q gas chromatography column to separate residual CO<sub>2</sub> from N<sub>2</sub>O. The N<sub>2</sub>O was then introduced into a Thermo Delta V Plus mass spectrometer via a ConFlo IV open split system, and measured for  $\delta^{15}\text{N}_{\text{bulk}}$ ,  $\delta^{18}\text{O}$ , and  $\delta^{15}\text{N}_{\alpha}$  by simultaneously monitoring  $m/z$  44, 45, 46 (N<sub>2</sub>O<sup>+</sup> molecular ions), and  $m/z$  30 and 31 (NO<sup>+</sup> fragment) for a single aliquot of air. The N<sub>2</sub>O mole fraction was determined on the same aliquot of air by relating the  $m/z$  44 peak area to known N<sub>2</sub>O mole fractions in whole air samples on the NOAA WMO scale (Hall et al., 2007).

Raw ion traces were integrated using a custom MATLAB script. Raw deltas were calculated relative to rectangular peaks generated by dipping the reference inlet into an open split flushed with pure N<sub>2</sub>O working reference gas of arbitrary isotopic composition. The calculation of delta values followed the formulation described by Kaiser and Röckmann (2008). The data reduction included a correction for <sup>17</sup>O isobaric interference, a correction for “scrambling” in the ion source (by which a fraction of ionized nitrogen atoms is rearranged between the terminal and central N atoms in N<sub>2</sub>O, i.e., about 8% of NO fragments include the terminal N), and calculation of  $\delta^{15}\text{N}_{\text{bulk}}$ ,  $\delta^{15}\text{N}_{\alpha}$ ,  $\delta^{15}\text{N}_{\beta}$  and  $\delta^{15}\text{N}^{\text{SP}}$ . A scrambling coefficient of 0.082, identical to that of Kaiser et al., 2004, was adopted for our data reduction. The assumption of the scrambling coefficient represents a source of uncertainty, so we explored the sensitivity of the data reduction to a wide range of scrambling coefficient values (Figure S3 in Supporting Information S1). The uncertainty introduced due to the scrambling coefficient is negligible over the range of reported scrambling coefficients (0.079–0.095) (Kaiser et al., 2004; Kelly et al., 2023).

To convert the raw delta values to delta values versus Air-N<sub>2</sub> and VSMOW, we adopted the one-point calibration routine outlined by Schilt et al. (2014). We made use of two cylinders of air from Niwot Ridge, Colorado, USA that were filled in December 2008 and September 1988. We refer to the tanks as NOAA1 and NOAA2, respectively. NOAA2 was used as a primary standard and was measured 4–6 times during a typical measurement series. The second cylinder, NOAA1, contained younger air and was measured against NOAA2 for verification (Figures S4 and S5 in Supporting Information S1). NOAA1 was previously used as a primary standard (Menking et al., 2020; Schilt et al., 2014) but was observed to have been contaminated, thus NOAA2 was adopted as the primary standard. The internal precision (1 $\sigma$ ) of our measurements on NOAA2 standard air was 0.44‰ for  $\delta^{15}\text{N}_{\alpha}$ , 0.57‰ for  $\delta^{15}\text{N}_{\beta}$ , 0.92‰ for  $\delta^{15}\text{N}^{\text{SP}}$ , 0.20‰ for  $\delta^{15}\text{N}_{\text{bulk}}$ , 0.38‰ for  $\delta^{18}\text{O}$ , and 2.69 nmol mol<sup>–1</sup> for N<sub>2</sub>O mole fraction over the duration of the measurement campaign (January 2020–June 2021).

We also compared measurements with University of East Anglia (UEA) and Portland State University. Unfortunately, due to a suspected (hydro) fluorocarbon interference from CF<sub>4</sub> on *m/z* 31, site-dependent isotope measurements could not be reliably measured at UEA. However, the bulk isotope measurements at UEA and OSU agreed within the analytical uncertainties. We also used calibration materials prepared at Portland State University to 430–540 nmol mol<sup>-1</sup> (in synthetic air) from N<sub>2</sub>O isotope reference gas obtained from the Swiss Federal Laboratories for Materials Science and Technology (EMPA) and calibrated by Tokyo Institute of Technology (TITech). Values are comparable within uncertainty except in a few cases (see Table S3 in Supporting Information S1).

Finally, the calibrated N<sub>2</sub>O mole fraction and isotope deltas were corrected for gravitational fractionation in firn using measurements of δ<sup>15</sup>N of molecular nitrogen (N<sub>2</sub>), as well as an apparent system “blank” determined from measurement of standard gas introduced over bubble-free ice and otherwise processed like the ice core samples. The apparent offsets from the assigned standard values were -2.3 nmol mol<sup>-1</sup> for N<sub>2</sub>O, +0.09‰ for δ<sup>15</sup>N<sub>bulk</sub>, -0.20‰ for δ<sup>18</sup>O, -0.24‰ for δ<sup>15</sup>N<sub>α</sub>, +0.42‰ for δ<sup>15</sup>N<sub>β</sub>, -0.66‰ for δ<sup>15</sup>N<sup>SP</sup>. We did not apply a correction to the isotope deltas for diffusive fractionation in the firn column. We estimate that diffusion in the firn during the fast rise in N<sub>2</sub>O during the last deglaciation could have contributed up to -0.04‰ to δ<sup>15</sup>N<sub>bulk</sub> and -0.08‰ to δ<sup>18</sup>O. Diffusive fractionation would not influence the site preference since isotopomers have the same mass.

## 2.2. WAIS Divide and Talos Dome Samples

WDC and TALDICE samples were analyzed at the University of Bern using the methods described by Schmitt et al. (2014) and Fischer et al. (2019). Ice samples of around 160 g were melted using infrared lamps. To minimize the dissolution of N<sub>2</sub>O in liquid water, the gas extraction was carried out first under vacuum and then under a constant helium (He) flow through the melt water. H<sub>2</sub>O vapor and CO<sub>2</sub> were removed from the released air with a cold trap and Ascarite, respectively. The remaining air sample was collected in an air trap cooled to -180°C. By heating the air trap to -78°C, the bulk air (N<sub>2</sub>, O<sub>2</sub>, Ar) was released and its volume was measured to determine the N<sub>2</sub>O mole fraction. The air trap was then heated to 100°C to release N<sub>2</sub>O, CH<sub>4</sub>, Xe and other organic trace gases into a separation line under continuous He flow. After a preconcentration step, the gases were separated on a gas chromatography column and injected successively into an Elementar IsoPrime isotope ratio mass spectrometer, where *m/z* 44, 45, and 46 were monitored. Isotope ratios were calculated relative to rectangular peaks produced by injection of pure N<sub>2</sub>O gas pulses from a reference inlet system. The delta values were calibrated to the international scales using a reference gas cylinder “Boulder” CA08289 from NOAA, filled in 2008, and measured daily before the sample run. The N<sub>2</sub>O mole fraction was determined by comparing the amount of N<sub>2</sub>O (reflected by the N<sub>2</sub>O peak area) to the amount of total air; this ratio was referenced to the N<sub>2</sub>O mole fraction of the “Boulder” air measurement. The measurement precision of N<sub>2</sub>O mole fraction, δ<sup>15</sup>N and δ<sup>18</sup>O is 3 nmol mol<sup>-1</sup>, 0.3‰ and 0.4‰ respectively.

WDC and TALDICE measurements were corrected for gravitational fractionation in firn using measurements of δ<sup>15</sup>N of molecular nitrogen (Eggleston et al., 2016) as well as for offsets between Bern and OSU labs determined by Schilt et al. (2014).

## 2.3. Data Quality and Agreement

We present measurements of N<sub>2</sub>O mole fraction and isotope deltas from 60 TG ice core samples containing air with 28 unique ages spanning the period 21.0–11.1 ka. 32 samples come from identical transect positions on TG and represent replicate measurements (analogous to depth-adjacent samples in ice cores with vertically oriented depth-age scales). We also present results from ice samples spanning the period 41.8–35.8 ka including 21 TG samples (15 unique ages, 6 replicates), 41 WDC samples, and 11 TALDICE samples. Replication of the TG samples allowed us to estimate analytical uncertainty and screen measurements for potential contamination by in situ N<sub>2</sub>O production (e.g., Miteva et al., 2016; Sowers, 2001).

The replication of N<sub>2</sub>O mole fraction in TG deglacial samples was poor for samples older than 15.6 ka, including samples dating to the Last Glacial Maximum (LGM). Three samples at 21.0, 19.4, and 16.1 ka had elevated N<sub>2</sub>O mole fractions (by 12–17 nmol mol<sup>-1</sup>) relative to replicate measurements. We suspect these samples were affected by excess N<sub>2</sub>O produced in situ and excluded them from further analysis. We justify excluding the elevated N<sub>2</sub>O measurements, but not other measurements, for four reasons. (a) Other samples agreed closely with published N<sub>2</sub>O data (Figure 1) (Fischer et al., 2019; Schilt et al., 2014). (b) Two of the samples older than 15.6 ka

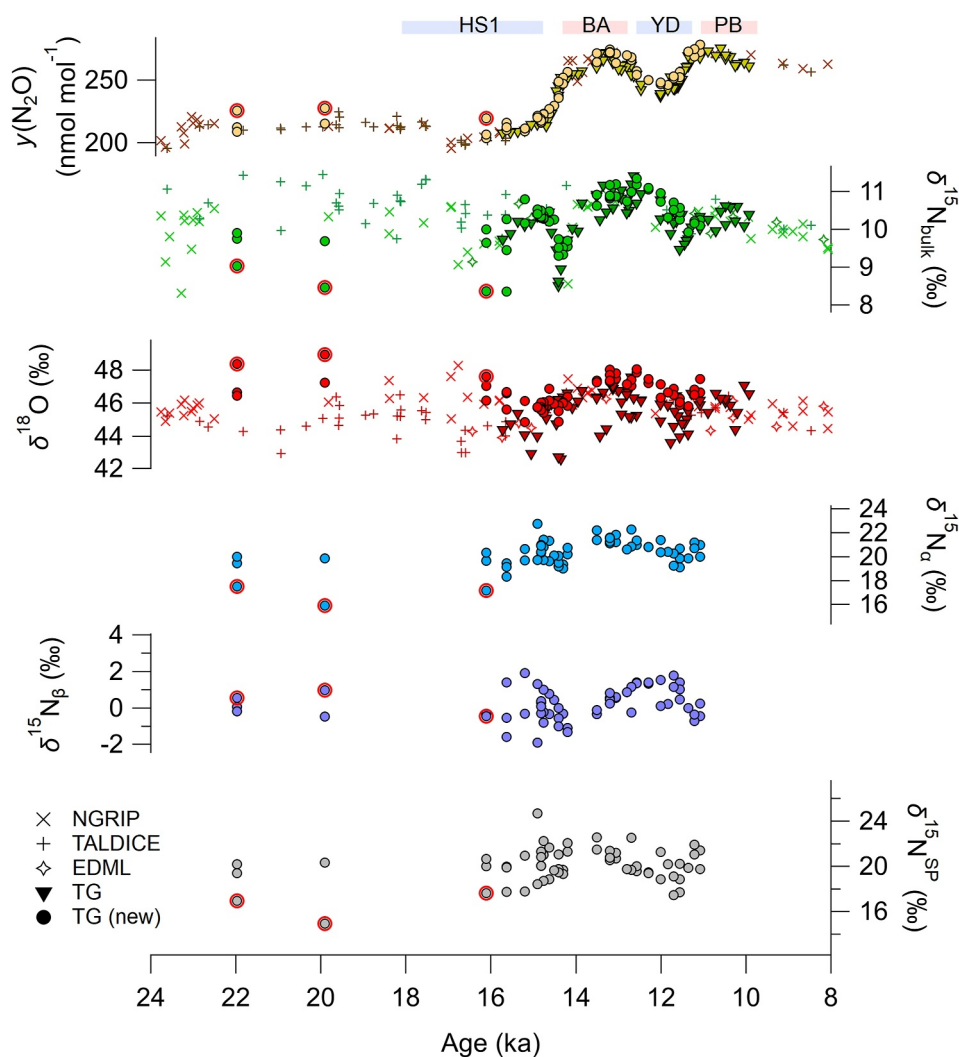


**Figure 1.** Ice core  $\text{N}_2\text{O}$  mole fraction and isotope data from Taylor Glacier (TG (new)) compared to existing records from North Greenland (NGRIP), Talos Dome (TALDICE), EPICA Dronning Maud Land (EDML) (Fischer et al., 2019), and Taylor Glacier (TG) (Schilt et al., 2014). Three samples at 21.0, 19.4, and 16.1 ka likely affected by in situ  $\text{N}_2\text{O}$  production are circled in red. The timing of Heinrich Stadial 1 (HS1), the Bølling-Allerød warming (BA), Younger Dryas cooling (YD), and Pre-Boreal warming (PB) are indicated at the top.

were measured in triplicate, and the  $\text{N}_2\text{O}$  measurements agreed within precision after excluding the elevated values. (c) The elevated  $\text{N}_2\text{O}$  samples consistently have low  $\delta^{15}\text{N}_{\text{bulk}}$ , high  $\delta^{18}\text{O}$ , and low  $\delta^{15}\text{N}^{\text{SP}}$  values relative to the replicates. (d) The samples with elevated  $\text{N}_2\text{O}$  mole fraction are associated with high dust content (Figure S6 in Supporting Information S1), which is hypothesized to stimulate in situ  $\text{N}_2\text{O}$  production as a result of biological denitrification when microbes on dust particles are in contact with nitrate deposited with the dust, or abiotic denitrification in the presence of ferrous iron (Miteva et al., 2016).

Other samples demonstrated poor replication in just one isotope signature but did not show the characteristic pattern of offsets for all isotope signatures as described above. For example, the data at 15.6 ka are scattered for  $\delta^{15}\text{N}_{\text{bulk}}$ , but reasonable agreement is found in  $\delta^{18}\text{O}$  and  $\text{N}_2\text{O}$  mole fractions (Figure 1). Another example is the poor agreement in  $\delta^{15}\text{N}^{\text{SP}}$  for the samples at 14.9 ka, but close agreement in  $\delta^{15}\text{N}_{\text{bulk}}$  and  $\text{N}_2\text{O}$  mole fraction. We do not know the reason(s) for these outliers and accept them as analytical uncertainty. The standard deviation ( $1\sigma$ ) of pooled replicate pairs (after removing three suspected of in situ produced  $\text{N}_2\text{O}$ ) is 3.1  $\text{nmol mol}^{-1}$  for  $\text{N}_2\text{O}$ , 0.3‰ for  $\delta^{15}\text{N}_{\text{bulk}}$ , 0.4‰ for  $\delta^{18}\text{O}$ , 0.7‰ for  $\delta^{15}\text{N}_{\alpha}$ , 0.8‰ for  $\delta^{15}\text{N}_{\beta}$ , 1.4‰ for  $\delta^{15}\text{N}^{\text{SP}}$ . This precision is similar to

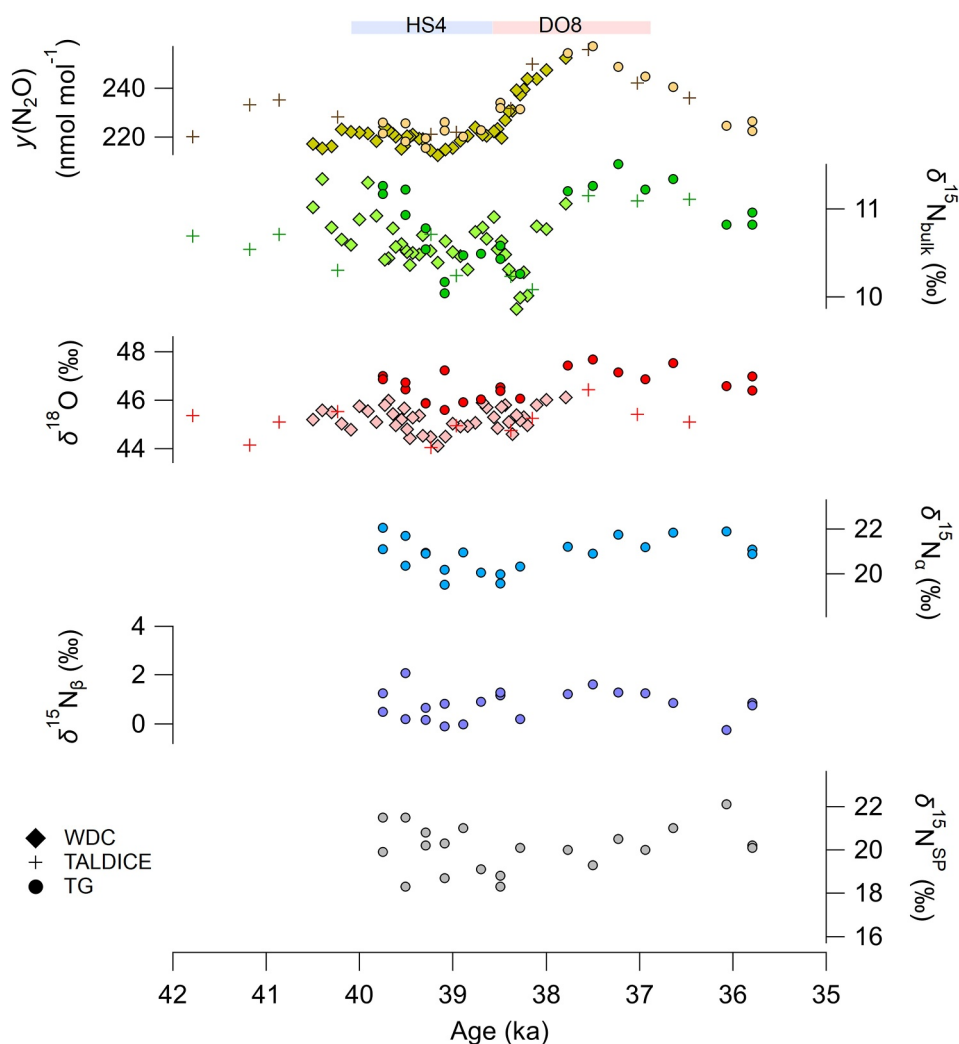


**Figure 2.** Ice core  $\text{N}_2\text{O}$  mole fraction and isotope data from Taylor Glacier (TG), West Antarctic Ice Sheet Divide (WDC), and Talos Dome (TALDICE) spanning the Heinrich Stadial 4/Dansgaard-Oeschger 8 interval.

or better than for previous ice core studies (Fischer et al., 2019; Park et al., 2012; Prokopiou et al., 2018; Schilt et al., 2014), in particular for  $\delta^{15}\text{N}^{\text{SP}}$  analysis.

The new  $\text{N}_2\text{O}$  mole fraction and  $\delta^{15}\text{N}_{\text{bulk}}$  data across the deglaciation agree well with existing data from Taylor Glacier, TALDICE, EDML, and NGRIP (Figure 1).  $\text{N}_2\text{O}$  mole fractions are close to existing data across the last deglaciation and during the LGM with a lowest measured  $\text{N}_2\text{O}$  mole fraction of  $201.6 \text{ nmol mol}^{-1}$ . Fischer et al. (2019) measured  $195.6 \text{ nmol mol}^{-1}$  at 16.9 ka, but we do not have ice samples at that age.  $\delta^{15}\text{N}_{\text{bulk}}$  does not reach values as low as existing TG data (Schilt et al., 2014) and one data point from the NGRIP ice core (14.5 ka) (Fischer et al., 2019), but the new  $\delta^{15}\text{N}_{\text{bulk}}$  values generally reproduce earlier data. The  $\delta^{15}\text{N}_{\text{bulk}}$  data also do not reach as low as existing data at the local minimum of the Younger Dryas (11.5 ka). The new  $\delta^{18}\text{O}$  data are elevated by  $1.0\text{‰}$  relative to the existing data. We do not know the reason for this offset, but differences in methods between OSU and UBern laboratories are likely the culprit, such as differences in the gas purification steps or calibration procedures.  $\delta^{18}\text{O}$  is not used in our subsequent analyses, and thus the offset is inconsequential for the interpretations that follow.

We also assess the quality and agreement of the new data spanning the HS4/DO8 transition (41.8–35.8 ka). Six replicates of the TG data agreed well except for one sample at 39.1 ka that had elevated  $\delta^{18}\text{O}$  (Figure 2).  $\text{N}_2\text{O}$  mole fraction and isotope signatures resembled the replicate sample, so we did not exclude it. The standard deviation ( $1\sigma$ ) of TG pooled replicate pairs across the HS4/DO8 interval is  $3.2 \text{ nmol mol}^{-1}$  for  $\text{N}_2\text{O}$ ,  $0.1\text{‰}$  for  $\delta^{15}\text{N}_{\text{bulk}}$ ,

0.5 ‰ for  $\delta^{18}\text{O}$  and  $\delta^{15}\text{N}_\alpha$ , 0.7‰ for  $\delta^{15}\text{N}_\beta$ , 1.2‰ for  $\delta^{15}\text{N}^{\text{SP}}$ . The TG  $\text{N}_2\text{O}$  mole fraction and  $\delta^{15}\text{N}_{\text{bulk}}$  data generally show close agreement with data from the WDC and TALDICE ice cores measured at the University of Bern (Figure 2). Similar to the deglacial data sets,  $\delta^{18}\text{O}$  is more enriched in TG samples by 1.0‰ relative to the UBern measurements on WDC and TALDICE samples. In general, the features resolved in the WDC data are similar to the TG data, though there are noticeable differences. The TG data resolve a sharper decrease in  $\delta^{15}\text{N}_{\text{bulk}}$  from 39.7 to 39.0 ka, while the WDC data are more scattered. Second, the WDC data resolve a sharp decrease in  $\delta^{15}\text{N}_{\text{bulk}}$  centered at 38.3 ka that is coincident with the onset of the rapid  $\text{CH}_4$  rise at DO8. This feature is not resolved in the TG data. The difference may be due to higher smoothing of the atmospheric signal due to slower bubble trapping in the firm at the TG accumulation zone as well as lower time resolution of the samples relative to WDC.

### 3. Results

#### 3.1. Spline Fits

To extract the low-frequency signals, we fitted smoothing splines to the  $\text{N}_2\text{O}$  mole fraction and isotope records (Enting, 1987). The spline fitting routine has commonly been applied to atmospheric and ice core data sets to illustrate temporal trends without bias from outliers (e.g., Fischer et al., 2019; Menking et al., 2020; Schilt et al., 2014). We chose a cutoff period of 1000 years for the smoothing splines because we found that this captured the long-term trends without introducing short-term variability not resolved by the data (Figure S8 in Supporting Information S1). For the deglacial interval, we began the smoothing spline fits at 16.1 ka in order to avoid fitting splines through the large data gaps from 21.0–19.4 to 19.4–16.1 ka. The data at 16.1 ka exhibit the lowest  $\text{N}_2\text{O}$  mole fraction in the new TG data set with isotope deltas similar to LGM values (Fischer et al., 2019), providing a good “starting point” for identifying trends spanning the  $\text{N}_2\text{O}$  rise. For  $\text{N}_2\text{O}$  mole fraction and  $\delta^{15}\text{N}_{\text{bulk}}$ , we fit splines to the combined data sets including new TG data, and existing TG, NGRIP, TALDICE, and EDML data. The routine generated 2,000 realizations of splines by randomly perturbing the data within a normal distribution described by the pooled  $1\sigma$  uncertainties. Previously published TG data from Schilt et al. (2014) were placed on an updated age scale (i.e., Baggenstos et al., 2017), which shifted the abrupt  $\text{N}_2\text{O}$  rise by about 0.2 ka younger relative to the original study and Fischer et al. (2019).

#### 3.2. Modeling $\text{N}_2\text{O}$ Source Emissions

To explore how the  $\text{N}_2\text{O}$  source emissions evolved across the last deglaciation and HS4/DO8, we generated plausible emissions histories by inversely solving for  $\text{N}_2\text{O}$  source changes using a two-box model constrained by the spline fits to the data. The analysis is run in a Monte Carlo framework that accounts for uncertainties in the data and model parameters including source  $\delta^{15}\text{N}_{\text{bulk}}$  and  $\delta^{15}\text{N}^{\text{SP}}$  signatures, atmospheric lifetime of  $\text{N}_2\text{O}$ , fractionation during stratospheric removal, and stratospheric-tropospheric exchange rate (Table 1). The model is identical to that used by Menking et al. (2020) and Schilt et al. (2014), but with isotope parameters adjusted to interpret site preference data. The calculation was run in two configurations: (a) to solve for the marine ( $E_{\text{mar}}$ ) versus terrestrial ( $E_{\text{ter}}$ ) fraction of  $\text{N}_2\text{O}$  emissions constrained by  $\text{N}_2\text{O}$  mole fraction and  $\delta^{15}\text{N}_{\text{bulk}}$  data, and (b) to solve for the nitrification ( $E_{\text{nit}}$ ) versus denitrification ( $E_{\text{den}}$ ) fraction of the total  $\text{N}_2\text{O}$  emissions constrained by  $\text{N}_2\text{O}$  mole fraction and  $\delta^{15}\text{N}^{\text{SP}}$  data.

Below, we present the changes in  $E_{\text{ter}}$ ,  $E_{\text{mar}}$ ,  $E_{\text{nit}}$  and  $E_{\text{den}}$ . We also show the absolute emissions in Section 3.7, which are more influenced by the model's choices of isotope signatures and initial source fractions and are therefore less precise. For the deglacial analysis of  $E_{\text{mar}}$  and  $E_{\text{ter}}$ , we combined the new data with existing published data and verified the trends already determined by Schilt et al. (2014) and Fischer et al. (2019). For this the starting fraction of  $E_{\text{mar}}$  to  $E_{\text{total}}$  was constrained to between 0.30 and 0.58 for the timestep at 27 ka (Table 1). The sensitivity of the results to this range of initial ocean fractions was tested by Fischer et al. (2019), and it was found that the major features and standard deviation of the results were robust to a larger range of starting fractions (25%–63%) that was likely too generous especially on the low end. Further, the mean preindustrial source fraction diagnosed by the model is quite near the preindustrial average determined independently by model studies (43%) (Battaglia & Joos, 2018). For the determination of  $E_{\text{den}}$  and  $E_{\text{nit}}$  using  $\delta^{15}\text{N}^{\text{SP}}$  data, no assumption was made about the starting source fraction. In other words, the model was allowed to freely explore the full parameter space as long as the determined initial fraction was between 0 and 1.

**Table 1**  
*Parameters Used in Source Modeling*

Parameter	Value, range and/or $1\sigma$ uncertainty	Mean $\pm 1\sigma$ value in ensemble	Description	Reference
$F_{TS}$	$[4.11 \times 10^{17}, 6.63 \times 10^{17}] \text{ kg a}^{-1}$	$5.4 \times 10^{17} \text{ kg a}^{-1}$	Tropospheric-stratospheric exchange rate	Ishijima et al. (2007)
$\tau_{\text{strat}}$	$(123 \pm 9) \text{ a}$	123 a	$\text{N}_2\text{O}$ lifetime in equilibrium	Prather et al. (2015)
$\epsilon(^{15}\text{N}^{\text{SP}})$	$(-14.1 \pm 1.8) \text{ ‰}$	$(-14.1 \pm 1.7) \text{ ‰}$ , $(-12.6 \pm 1.4) \text{ ‰}^{\text{a}}$	Site preference removal fractionation	Toyoda et al. (2001)
$\epsilon(^{15}\text{N}_{\text{bulk}})$	$(-16.8 \pm 1.6) \text{ ‰}$	$(-17 \pm 1.6) \text{ ‰}$	Bulk isotope removal fractionation	Röckmann et al. (2001), Toyoda et al. (2001), Yung and Miller (1997)
$n_{\text{atm}}$	$1.77 \times 10^{20} \text{ mol}$		Amount of air in atmosphere	Röckmann et al. (2003)
$X_{\text{strat}}$	0.15		Stratosphere mass fraction of whole atmosphere	Röckmann et al. (2003)
$\delta_{\text{nit}}^*(^{15}\text{N}^{\text{SP}})$	$[19.6, 36.6] \text{ ‰}$	$(28.1 \pm 4.1) \text{ ‰}$ , $(27.8 \pm 4.9) \text{ ‰}^{\text{a}}$	Nitrification (and fungal denitrification) source site preference	Toyoda et al. (2017)
$\delta_{\text{den}}(^{15}\text{N}^{\text{SP}})$	$[-10.7, 0.1] \text{ ‰}$ , $[4.2, 15.1] \text{ ‰}^{\text{a}}$	$(-4.9 \pm 2.9) \text{ ‰}$ , $(6.6 \pm 2.2) \text{ ‰}^{\text{a}}$	Denitrification source site preference (pure culture)	Toyoda et al. (2017)
$\delta_{\text{ter}}(^{15}\text{N}_{\text{bulk}})$	$[-34, 2] \text{ ‰}$	$(-16.5 \pm 3.9) \text{ ‰}$	Terrestrial source bulk isotopic composition	Kim and Craig (1993), Snider et al. (2015), Toyoda et al. (2017)
$\delta_{\text{mar}}(^{15}\text{N}_{\text{bulk}})$	$[4, 12] \text{ ‰}$	$(7.2 \pm 1.7) \text{ ‰}$	Marine source bulk isotopic composition	Frame et al. (2014), Kim and Craig (1993), Toyoda et al. (2017)
$f_{\text{mar}}(t = 0)$	$[0.30, 0.58]$	$(0.43 \pm 0.09)$	Marine emissions starting fraction of total emission ( $t = 27 \text{ ka}$ )	Battaglia and Joos (2018), Fischer et al. (2019)
$f_{\text{nit}}^*(t = 0)$	$[0, 1]$	$(0.35 \pm 0.1)$	Nitrification (with possible fungal denitrification) starting fraction of total emissions	

<sup>a</sup>Values are shifted in a model run that accounts for 92% reduction of  $\text{N}_2\text{O}$  produced by denitrification with resulting isotopic enrichment.

One complication with a two end member analysis is that the  $\delta^{15}\text{N}^{\text{SP}}$  of  $\text{N}_2\text{O}$  produced by nitrifying microbes overlaps with that of denitrifying fungi (Toyoda et al., 2017; Yu et al., 2020) (Figures S1 and S2 in Supporting Information S1). The overall contribution of fungal denitrification to global atmospheric  $\text{N}_2\text{O}$  is unknown and debated (Rohe et al., 2021). Inhibitor studies suggest a potentially large role (Laughlin & Stevens, 2002), and genetic studies suggest only modest contributions (Bösch et al., 2023). Because we cannot distinguish fungal denitrification from bacterial nitrification using  $\delta^{15}\text{N}^{\text{SP}}$ , we refer to  $E_{\text{nit}}$  for the remainder of this manuscript as  $E_{\text{nit}}^*$ , denoting possible contribution to this end member from fungal denitrification.

Another complication with the two end member analysis is that in denitrifying marine and terrestrial environments,  $\text{N}_2\text{O}$  is reduced to  $\text{N}_2$  with isotope discrimination against the heavy and central isotopes (Scheer et al., 2020; Yamagishi et al., 2007). This leaves the remaining  $\text{N}_2\text{O}$  pool, that is, the  $\text{N}_2\text{O}$  that is ultimately emitted to the atmosphere, enriched in  $\delta^{15}\text{N}^{\text{SP}}$  relative to the pure culture end member values characterizing production (Figure S2 in Supporting Information S1). To estimate the effect of  $\text{N}_2\text{O}$  reduction, we performed model runs with adjusted isotope end member values for the denitrification source to account for site preference enrichment due to fractionation during  $\text{N}_2\text{O}$  reduction. It was recently determined that about 92% of the terrestrial  $\text{N}_2\text{O}$  produced by denitrification was reduced to  $\text{N}_2$  (Scheer et al., 2020). The fractionation factor of  $\text{N}_2\text{O}$  reduction is  $-5.9\text{ ‰}$  (Yu et al., 2020), which results in a range of  $\delta^{15}\text{N}^{\text{SP}}$  shifted upwards about 15‰ if the pure culture end member values are recalculated following:

$$\delta_{\text{residual}} = \delta_{\text{original}} + \epsilon^{15}\text{N}^{\text{SP}} \times \ln(r\text{N}_2\text{O}) \quad (2)$$

where  $r\text{N}_2\text{O}$  is the ratio of residual to total  $\text{N}_2\text{O}$  and  $\epsilon^{15}\text{N}^{\text{SP}}$  is the fractionation factor. The influence of this on the determined contribution of denitrification to the global  $\text{N}_2\text{O}$  budget is discussed below.

Our model routine also produced a set of results demonstrating the expected  $\delta^{15}\text{N}_{\text{bulk}}$  and  $\delta^{15}\text{N}^{\text{SP}}$  in the case where the fraction of sources did not change and any variations were due to atmospheric imbalance between the

tropospheric source and stratospheric sink. This represents a null hypothesis against which to compare the results. Below we describe trends in the deglacial and HS4/DO8 data sets as resolved by the spline fits, highlight major features in the evolution of the  $N_2O$  sources including determination of  $E_{nit}^*$  versus  $E_{den}$  contribution to global  $N_2O$ , and discuss the implications of  $N_2O$  emissions changes in light of global climate and the nitrogen cycle.

### 3.3. Data Trends: Deglacial Rise 16.1–11.1 ka

A fundamental observation is that the  $N_2O$  site preference data did not exhibit a step-like change from the LGM (21–16 ka) to the early Holocene (11 ka). The  $\delta^{15}N^{SP}$  data suggest a LGM average site preference value of about 20‰, equal to the early Holocene value. For context, the site preference in the period 2000–2008 CE has been measured as  $(18.9 \pm 2.4)$ ‰ (Park et al., 2012) and  $(18.3 \pm 0.5)$ ‰ (Ghosh et al., 2023; Toyoda et al., 2013). The temporal  $\delta^{15}N^{SP}$  changes during the last deglaciation are small relative to the noise. The spline fits act as a low-pass filter on the data and offer a means to identify variations during the  $N_2O$  rise and judge their significance. In fact, few variations resolved in the  $\delta^{15}N^{SP}$  data demonstrate changes significant above the  $2\sigma$  uncertainty of the spline fits (Figure 3). We highlight two main features in the new data: (a) During the interval 16.1–13.2 ka,  $N_2O$  mole fraction gradually increased by  $14 \text{ nmol mol}^{-1}$  from 16.1–14.7 ka, rapidly increased by  $35 \text{ nmol mol}^{-1}$  at the Bolling-Allerod warming, and then continued to increase more gradually by  $16 \text{ nmol mol}^{-1}$ . The largest change in  $\delta^{15}N^{SP}$  during this interval was an increase from  $(19.2 \pm 1.5)$ ‰ at 15.5 ka to  $(21.9 \pm 1.6)$ ‰ at 13.7 ka. (b) During the interval 13.2–11.1 ka,  $N_2O$  mole fraction decreased by  $26 \text{ nmol mol}^{-1}$  with the Younger Dryas cold period and subsequently recovered by  $29 \text{ nmol mol}^{-1}$  by 11.1 ka.  $\delta^{15}N^{SP}$  decreased from  $(21.9 \pm 1.6)$ ‰ at 13.7 ka to  $(19.0 \pm 1.1)$ ‰ at 11.7 ka and subsequently recovered to  $(21.1 \pm 1.3)$ ‰ by 11.1 ka (Figure 3).

Unfortunately, there is a data gap between 14.2–13.5 ka, which was avoided during sampling the TG transect because of a disturbance in the ice stratigraphy (Schilt et al., 2014). We used a “bootstrapping” method to test the sensitivity of the features in our spline fits to exclude the data points at 14.2 and 13.5 ka. We found that the spline fits after removing one or the other of those data points reaches a slightly lower site preference maximum at 13.7 ka of around 21.5‰, but the main features of the data including the overall upward trend from 15.5–13.7 ka and local minimum at 14.5 ka were preserved (Figure S9 in Supporting Information S1).

There are also smaller variations in the new  $\delta^{15}N^{SP}$ . For instance, there is a local maximum in  $\delta^{15}N^{SP}$  at 14.9 ka and a slight decreasing trend from 14.9 to 14.5 ka that results in a local minimum occurring simultaneously with the minimum in  $\delta^{15}N$  and the rapid  $N_2O$  rise. This feature is in the right direction to attribute to tropospheric-stratospheric imbalance (Figure S10 in Supporting Information S1) (Tans, 1997), but we do not favor this interpretation because we do not see a similar feature reflected in  $\delta^{18}O$  (Figure 1).

### 3.4. Sources: Deglacial Rise 16.1–11.1 ka

The  $N_2O$  site preference record from TG ice core samples provides a novel way to constrain how the microbial pathways of global  $N_2O$  emissions changed during the  $N_2O$  rise at the last deglaciation. As noted above, the deglacial interval does not exhibit a notable shift in  $\delta^{15}N^{SP}$  between glacial and interglacial times. The modeling suggests approximately equal contributions of increasing  $E_{nit}^*$  and  $E_{den}$  drove the deglacial  $N_2O$  rise (Figure 3).  $E_{den}$  increased by  $(1.4 \pm 0.5) \text{ Tg a}^{-1}$  (all fluxes are given as N equivalents) and  $E_{nit}^*$  increased by  $(1.5 \pm 0.5)$  between 16.1–13.2 ka with  $E_{nit}^*$  reaching a local maximum about 500 years before  $E_{den}$ . Assuming a more enriched end member value to account for reduction and isotope enrichment of the  $N_2O$  pool during denitrification modestly changes the results with increases of  $(2.0 \pm 0.7) \text{ Tg a}^{-1}$  for  $E_{den}$  and  $(1.2 \pm 0.7) \text{ Tg a}^{-1}$  for  $E_{nit}^*$  (Figure 3).

Previous studies have emphasized the intensification of marine denitrification in the global nitrogen cycle during the last deglaciation (Galbraith et al., 2013; Ganeshram et al., 2000), but the implication of  $\delta^{15}N^{SP}$  record and analysis is, at least for atmospheric  $N_2O$ , that denitrification cannot be the full story. The mechanism for the shift from low  $N_2O$  characteristic of a cold glacial climate to high  $N_2O$  characteristic of a warm, interglacial climate was not an increase in emissions from a single pathway; rather, both nitrification (and possibly fungal denitrification) and denitrification pathways appear sensitive to shifts in global climate. From the marine perspective, our results are consistent with proxy data demonstrating expanding hypoxic regions in the upper ocean during the deglaciation (Jaccard & Galbraith, 2012; Jaccard et al., 2014; Moffitt et al., 2015) and also do not preclude recent work using earth system models that showed that the deep ocean was less oxygenated during the LGM (Cliff et al., 2021). The deglacial ocean shifted from a sluggish AMOC with more stratified deep ocean, less primary

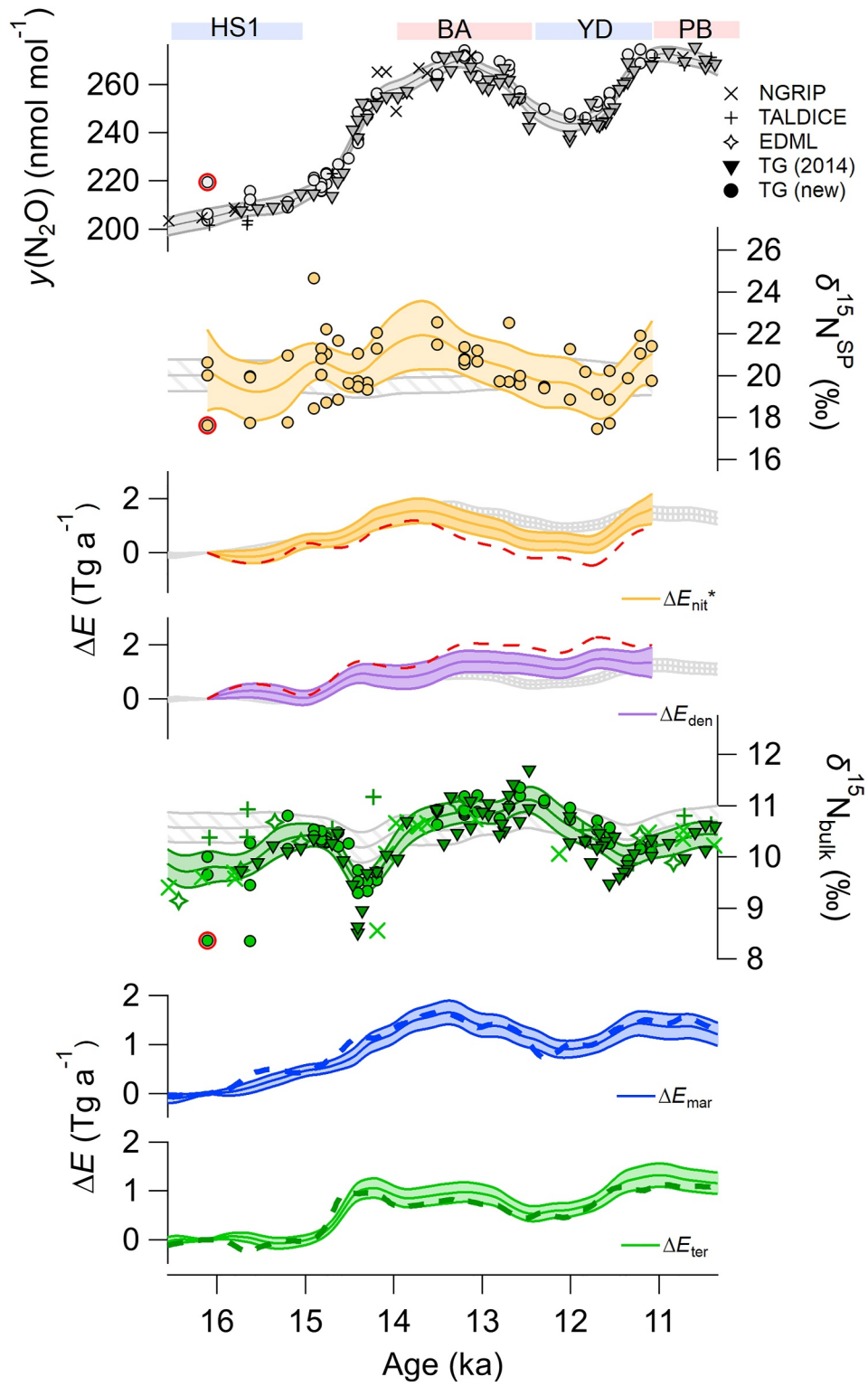


Figure 3.

productivity, and well-oxygenated surface waters that kept N<sub>2</sub>O emissions lower to an interglacial ocean with more productive surface waters and more surface ocean hypoxia with increased N<sub>2</sub>O emissions. Our data demonstrate that a significant shift in the balance of  $E_{\text{nit}}^*$  versus  $E_{\text{den}}$  is not a requisite of an accelerating AMOC, but one caveat to keep in mind when interpreting the source histories is that our analysis determined total  $E_{\text{nit}}^*$  and  $E_{\text{den}}$  globally without the ability to parse the pathway specifically to marine versus terrestrial ecosystems.

To this end, the model calculations of  $E_{\text{mar}}$  and  $E_{\text{ter}}$  changes may offer some guidance. Our marine and terrestrial emission histories closely resemble those of Fischer et al. (2019), who showed that roughly equal increases in  $E_{\text{mar}}$  and  $E_{\text{ter}}$  caused the deglacial N<sub>2</sub>O rise (Figure 3) (Fischer et al., 2019; Schilt et al., 2014). Given that our calculations also show roughly equal increases in  $E_{\text{nit}}^*$  and  $E_{\text{den}}$ , a simple conclusion is that denitrification remained the dominant pathway for N<sub>2</sub>O emitted from land (Vilain et al., 2014), and nitrification remained the dominant pathway for N<sub>2</sub>O emitted from the ocean (Freing et al., 2012), with the two increasing proportionally together. This pattern is broadly reflected in the similarities between the marine and nitrification source histories, and the land and denitrification source histories (Figure 3). Marine emissions are strongest in hypoxic regions such as the Eastern Tropical North Pacific, and the gradual increase in marine nitrification emissions reflected in our source histories are consistent with the expansion of hypoxic regions with maximum hypoxic extent occurring in the Bølling-Allerød (Jaccard & Galbraith, 2012). The fast increase in  $E_{\text{ter}}$  from 15–14.2 ka, a feature noted in previous studies (e.g., Fischer et al., 2019; Schilt et al., 2014), is mirrored by an equally rapid increase in  $E_{\text{den}}$ , and a slight flattening of the  $E_{\text{mar}}$  and  $E_{\text{nit}}^*$  emissions curves. Terrestrial N<sub>2</sub>O emissions are highly sensitive to soil moisture and temperature (Xu et al., 2012), and this fast rise in terrestrial emissions has been linked to shifts in the intertropical convergence zone and enhanced precipitation over the low-latitude tropics (Fischer et al., 2019; Rhodes et al., 2015). Our new results demonstrate that the fast ( $1.0 \pm 0.2$ ) Tg a<sup>-1</sup> increase in land emissions could have come predominantly from an acceleration of denitrification on land. The rapid increase in denitrification accounts for about ( $0.9 \pm 0.3$ ) Tg a<sup>-1</sup>, well within the uncertainties of the total land increase, though we cannot rule out some additional acceleration of nitrification on land.

The decrease in N<sub>2</sub>O emissions associated with the Younger Dryas cold period 13.2–12.0 ka was almost exclusively driven by a decrease in the nitrification (and potentially fungal denitrification) pathway.  $E_{\text{nit}}^*$  decreased by ( $1.0 \pm 0.3$ ) Tg a<sup>-1</sup> with only ( $0.3 \pm 0.3$ ) Tg a<sup>-1</sup> decrease from  $E_{\text{den}}$ . Similarly, the recovery from the Younger Dryas cooling saw N<sub>2</sub>O increase by 28 nmol mol<sup>-1</sup> from 12.0–11.1 ka, driven exclusively by ( $1.2 \pm 0.5$ ) Tg a<sup>-1</sup> increase in  $E_{\text{nit}}^*$ . The changes in  $E_{\text{nit}}^*$  are in the same direction and slightly larger when accounting for isotopic shifts in the denitrification end member due to reduction (total decrease in  $E_{\text{nit}}^*$  of ( $1.4 \pm 0.5$ ) Tg a<sup>-1</sup>). Schilt et al. (2014) and Fischer et al. (2019) suggested decreases in both terrestrial and marine emissions during the Younger Dryas cold interval, and the new source histories show a similar pattern with about ( $0.7 \pm 0.2$ ) Tg a<sup>-1</sup> decrease due to declining  $E_{\text{mar}}$  and about ( $0.4 \pm 0.2$ ) Tg a<sup>-1</sup> due to  $E_{\text{ter}}$ . This is the only interval in the new deglacial data set where the changes in  $E_{\text{nit}}^*$  and  $E_{\text{den}}$  depart significantly (beyond the 1 $\sigma$  uncertainties) from a scenario where  $E_{\text{mar}}$  is dominated by nitrification and  $E_{\text{ter}}$  is dominated by denitrification and the  $E_{\text{nit}}^*$  and  $E_{\text{den}}$  curves essentially resemble  $E_{\text{mar}}$  and  $E_{\text{ter}}$ , respectively (Figure 3). The model results show the decrease in  $E_{\text{nit}}^*$  exceeds the decrease in  $E_{\text{mar}}$  from 12.8–11.8 ka, potentially implicating a sensitivity of terrestrial nitrification to the YD cooling. The Younger Dryas cold interval is hypothesized to have been driven by a slowdown of the AMOC in response to a release of freshwater into the North Atlantic (Tarasov & Peltier, 2005). Marine N<sub>2</sub>O emissions during the Younger Dryas interval were investigated in an earth system model that tracks marine N<sub>2</sub>O production by nitrification and denitrification pathways (Joos et al., 2019). Freshwater forcing of AMOC drove a ( $0.7 \pm 0.2$ ) Tg a<sup>-1</sup> decrease in marine N<sub>2</sub>O emissions, similar to the total magnitude of N<sub>2</sub>O emissions change found by (Fischer et al., 2019). The decrease was driven almost completely by decreases in ocean nitrification as a result of O<sub>2</sub> changes in the low-latitude thermocline. The data presented in this study support this model result and

**Figure 3.** Spline fits to combined deglacial ice core data and calculated emission changes. Spline fits to N<sub>2</sub>O mole fraction and  $\delta^{15}\text{N}^{\text{SP}}$  were used to calculate the change in N<sub>2</sub>O emissions from nitrification ( $\Delta E_{\text{nit}}^*$  with possible contribution from fungal denitrification) and denitrification ( $\Delta E_{\text{den}}$ ). Spline fits to N<sub>2</sub>O mole fraction and  $\delta^{15}\text{N}_{\text{bulk}}$  were used to calculate the change in N<sub>2</sub>O emissions from marine ( $\Delta E_{\text{mar}}$ ) and terrestrial ( $\Delta E_{\text{ter}}$ ) sources. The marine and land N<sub>2</sub>O emission changes from Fischer et al. (2019) are plotted with dashed blue and green lines for comparison. The uncertainty bands represent 2 $\sigma$  of the full ensemble of spline fits to the data and 1 $\sigma$  of the calculated source changes. Gray bands with diagonal lines show the expected deltas and 1 $\sigma$  uncertainty assuming that the fraction of emissions does not change. Gray bands with vertical lines demonstrate the expected  $\Delta E_{\text{nit}}^*$  and  $\Delta E_{\text{den}}$  emissions changes for a “null hypothesis” in which nitrification (and possibly fungal denitrification) remained the dominant production pathway in the ocean, and denitrification remained dominant on land. Dashed red lines show the results if the end member range of isotopic values for denitrification is adjusted +15‰ for 92% reduction of N<sub>2</sub>O.

the notion that N<sub>2</sub>O production by marine denitrification is relatively insensitive to AMOC changes during the Younger Dryas (Joos et al., 2019).

### 3.5. Data Trends: HS4/DO8 41.8–35.8 ka

Data from the interval 41.8–35.8 ka provide the first opportunity to look at how N<sub>2</sub>O isotopes evolved across the HS4/DO8 transition. HS4/DO8 was a millennial-scale climate event during the last glacial period characterized by a cool Northern Hemisphere and gradual warming in the Southern Hemisphere, followed by an abrupt shift to warmer Northern Hemisphere climate and gradual Southern Hemisphere cooling. This “bipolar” antiphase behavior is a common feature of the last glacial climate recorded in ice cores and is thought to be driven by large-scale changes in AMOC (Buizert, Adrian, et al., 2015; Buizert et al., 2018; Stocker & Johnsen, 2003) with accompanying changes in the hydrological cycle on land (Rhodes et al., 2015; Wang et al., 2001). Our new data offer a perspective on millennial-scale climate variability to identify similarities and contrast differences to the data spanning the full deglacial N<sub>2</sub>O rise.

Smoothing splines were fit to the TALDICE, WDC, and TG ice core data by a similar routine as for the deglacial data (Figure 4). N<sub>2</sub>O mole fraction reached a minimum of 219 nmol mol<sup>-1</sup> at 39.3 ka during HS4, increased to a maximum of 256 nmol mol<sup>-1</sup> at 37.6 ka during the peak of DO8, and decreased to 224 nmol mol<sup>-1</sup> by 35.8 ka.  $\delta^{15}\text{N}_{\text{bulk}}$  decreased during HS4 (40.5–39.1 ka) by about  $(0.4 \pm 0.2) \text{‰}$ .  $\delta^{15}\text{N}_{\text{bulk}}$  reached a minimum of  $(10.3 \pm 0.2) \text{‰}$  at 38.3 ka, about midway through the rapid N<sub>2</sub>O rise at the DO8 warming. At the onset of DO8, as marked by the rapid 130 nmol mol<sup>-1</sup> increase in CH<sub>4</sub> (38.4 ka), N<sub>2</sub>O had already gradually risen by 11 nmol mol<sup>-1</sup> from the stadial minimum but increased at a higher rate at the DO onset. N<sub>2</sub>O continued to rise through the interstadial by 24 nmol mol<sup>-1</sup> before beginning to decrease at 36.5 ka. The  $\delta^{15}\text{N}_{\text{bulk}}$  data show an increase of  $(1.1 \pm 0.4) \text{‰}$  occurring during the sharpest N<sub>2</sub>O rise from 38.2–37.3 ka.

Changes in  $\delta^{15}\text{N}^{\text{SP}}$  were generally small relative to the measurement uncertainty, but spline fits resolved a decrease of  $(1.8 \pm 1.0) \text{‰}$  during the stadial (39.8–38.5 ka) including a local minimum centered at 38.5 ka (near the minimum in  $\delta^{15}\text{N}_{\text{bulk}}$  and the beginning of the abrupt N<sub>2</sub>O rise), and an increase of  $(2.9 \pm 1.9) \text{‰}$  during the interstadial (38.5–36.3 ka). The increase in  $\delta^{15}\text{N}^{\text{SP}}$  appeared to increase in two phases with a 1.0‰ increase occurring during the abrupt N<sub>2</sub>O rise and further increasing by 1.9‰ as N<sub>2</sub>O mole fraction decreased between 37.6–35.8 ka, though the latter feature is somewhat dependent on a single data point at 36.0 ka and is attenuated in bootstrapping experiments where this data point is excluded (Figure S11 in Supporting Information S1).

### 3.6. Sources: HS4/DO8 41.8–35.8 ka

We calculated source histories similar to the deglacial interval. We used N<sub>2</sub>O mole fraction and  $\delta^{15}\text{N}_{\text{bulk}}$  data to constrain the changes in  $E_{\text{mar}}$  and  $E_{\text{ter}}$ , and separately, we used the  $\delta^{15}\text{N}^{\text{SP}}$  and N<sub>2</sub>O mole fractions to constrain the changes in  $E_{\text{nit}}^*$  and  $E_{\text{den}}$ .

The results show that the stadial (40.5–39.1 ka) was characterized by slightly increasing N<sub>2</sub>O emissions on land ( $+0.1 \pm 0.1 \text{ Tg a}^{-1}$ ) with decreasing marine emissions (Figure 4). However, the slow rise in N<sub>2</sub>O mole fraction beginning at 39.3 ka was driven by increasing  $E_{\text{mar}}$  (additional  $(0.2 \pm 0.1) \text{ Tg a}^{-1}$ ).  $E_{\text{mar}}$  and  $E_{\text{ter}}$  rapidly increased around 38.7 ka by  $(0.9 \pm 0.2) \text{ Tg a}^{-1}$  and  $(0.5 \pm 0.2) \text{ Tg a}^{-1}$ , respectively, with  $E_{\text{ter}}$  responding slightly faster, reaching a maximum about midway through the N<sub>2</sub>O rise. Decreasing N<sub>2</sub>O mole fractions during the interstadial (37.5–35.8 ka) were driven by decreases in both  $E_{\text{ter}}$  and  $E_{\text{mar}}$ , which essentially declined back to stadial levels within 2 millennia in parallel to reconstructed Greenland temperatures.

The changes in the microbial pathways of N<sub>2</sub>O production determined from our  $\delta^{15}\text{N}^{\text{SP}}$  data demonstrate that the rapid N<sub>2</sub>O rise from HS4 to DO8 beginning around 38.7 ka was driven by a  $(0.6 \pm 0.3) \text{ Tg a}^{-1}$  increase in  $E_{\text{den}}$ , and  $(0.7 \pm 0.3) \text{ Tg a}^{-1}$  increase in  $E_{\text{nit}}^*$ . The full increase in  $E_{\text{den}}$  is about  $(1.0 \pm 0.4) \text{ Tg a}^{-1}$  from 39.75 to 37.6 ka. Assuming a more enriched end member for  $E_{\text{den}}$  to account for N<sub>2</sub>O reduction results in very similar source changes across the abrupt N<sub>2</sub>O rise ending at 37.6 ka with  $E_{\text{den}}$  increasing more overall across the full HS4/DO8 interval  $(1.6 \pm 0.6) \text{ Tg a}^{-1}$ .

The increase in marine nitrification- (and denitrification-) sourced N<sub>2</sub>O is likely due to AMOC resumption (Henry et al., 2016) re-invigorating the nitrogen cycle as nutrients stored in the deep ocean became more well-distributed through the surface and thermocline (Schmittner & Galbraith, 2008). Our model results show that  $E_{\text{den}}$  remained rather constant during the rapid increase in terrestrial and marine sources at the onset of DO8, pointing to

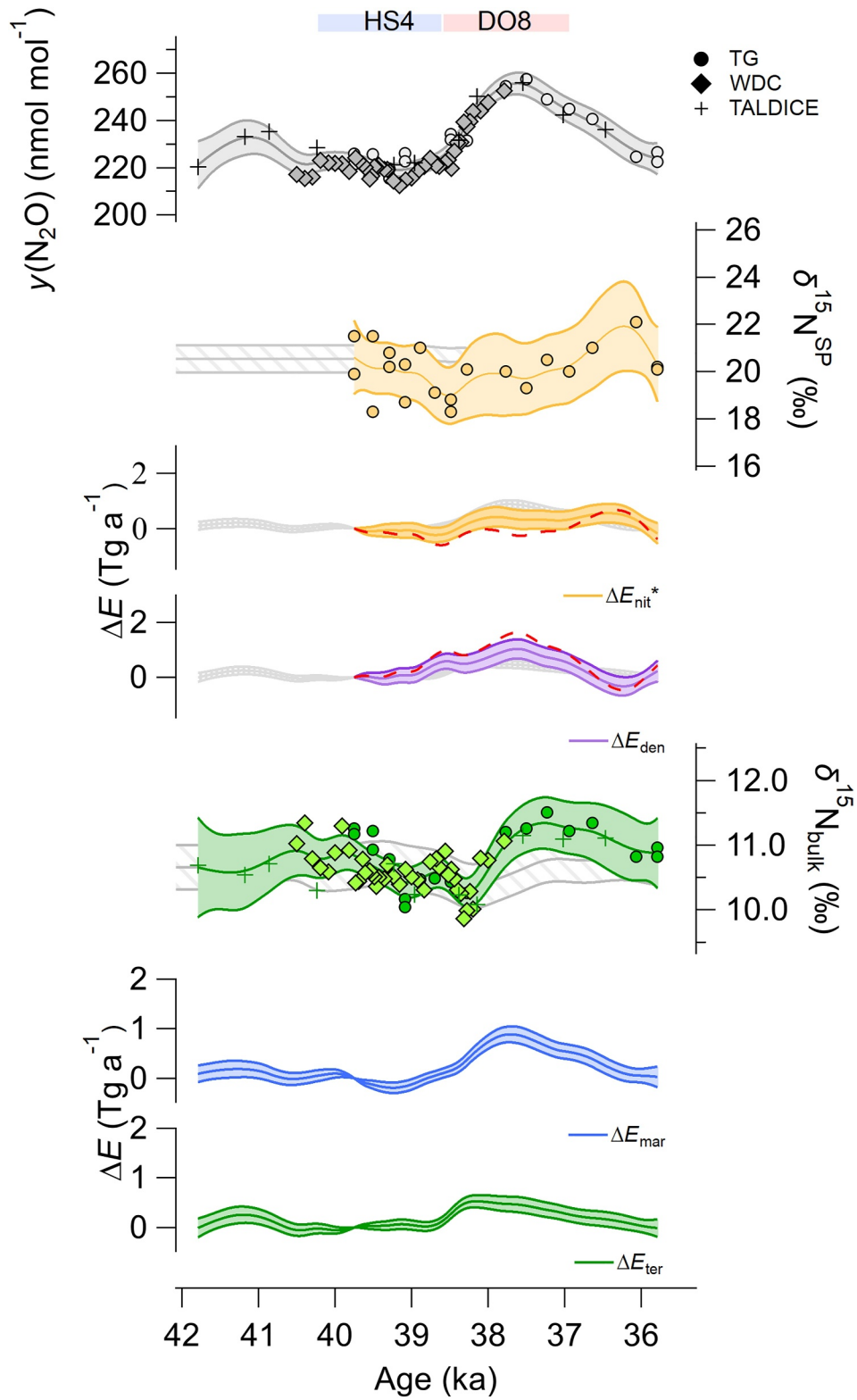


Figure 4.

nitrification (with possible contribution from fungal denitrification) being the main cause of both terrestrial and marine emission increases. The decrease in  $N_2O$  mole fraction beginning at 37.6 ka was caused predominantly by decreases in  $E_{den}$  with  $E_{nit}^*$  persisting or perhaps even accelerating slightly at 37.1 ka. This is the only instance in our HS4/DO8 reconstruction where the  $E_{nit}^*$  and  $E_{den}$  changes approach significant ( $1\sigma$ ) deviation from the expected trajectory if nitrification remained the dominant emissions pathway in the ocean and denitrification remained dominant on land (Figure 4). However, given the low data resolution and the dependence of the magnitude of  $E_{den}$  decrease on the data point at 36 ka (Figure S11 in Supporting Information S1), we refrain from interpreting this.

### 3.7. Absolute Source Emissions Histories

So far, we have only reported relative changes in  $N_2O$  emissions diagnosed by the model since our isotope data provide more precise constraints. The absolute emission histories are more uncertain given the high dependency on model parameters including isotopic values assigned to the source end members as well as starting source fractions. To demonstrate these uncertainties in hopes to spur future work on  $N_2O$  isotopes and global source reconstructions, we compare the absolute emissions histories diagnosed by the model for the case where denitrification end member  $\delta^{15}N^{SP}$  values are based on values from pure culture studies versus values that are enriched due to reduction of  $N_2O$  to  $N_2$  (see Table 1).

The result for both the deglacial and HS4/DO8 intervals is that denitrification, when considering isotopic enrichment of the residual  $N_2O$  pool, represents a higher contribution to total  $N_2O$  emissions (making up about 90% of total emissions) compared to the result using pure production isotope values (Figure 5). We find this implausible given that denitrification was estimated to only contribute 4.5% of total marine emissions during the preindustrial era (Battaglia & Joos, 2018), and our measured site preference values are not very different from preindustrial values. Since marine emissions make up 40%–50% of total  $N_2O$  emissions (based on bulk isotope source apportionment), denitrification would have to account for about 75% of marine emissions in addition to all land emissions. This disagrees with in situ flux estimates showing that most ocean  $N_2O$  production is from nitrification (Freing et al., 2012). On the other hand, we find it implausible that the  $\delta^{15}N^{SP}$  value of  $N_2O$  produced by denitrification and ultimately emitted to the atmosphere retains its pure culture  $\delta^{15}N^{SP}$  value given clear evidence that most of the  $N_2O$  produced by denitrification is reduced to  $N_2$  with fractionation that enriches the residual  $N_2O$  pool (Buchen et al., 2018; Lewicka-Szczepak et al., 2020; Scheer et al., 2020; Well et al., 2005, 2012; Yamagishi et al., 2007). Thus, our analysis reveals a mismatch in the global  $N_2O$  isotope budget that is likely due to a combination of errors in isotopomer signatures and other model parameters. To improve the prospect of future  $N_2O$  budget reconstructions using ice core data, we suggest that in addition to reducing uncertainties in source isotopic signatures, future modeling and flux work should also focus on parsing the relative contribution of nitrification versus denitrification in terrestrial and marine environments to atmospheric  $N_2O$  emissions.

## 4. Comparing Millennial-Scale $N_2O$ Change During HS4/DO8 and the Last Deglaciation

Our reconstructions allow us to compare the millennial-scale variations in the drivers of  $N_2O$  emissions during the HS4/DO8 transition to those spanning the full deglacial transition. A key similarity is that marine and terrestrial emissions were important for driving increases and decreases in atmospheric  $N_2O$  during both intervals, highlighting the sensitivity of the nitrogen cycle to climate change in both ecosystems (Figure 6). The reconstructions also demonstrate that this climate sensitivity is not unique to nitrification or denitrification; rather, both microbial pathways broadly speaking produce more  $N_2O$  in response to warming. Another key similarity is that land emissions appear to respond faster to warming at both the HS1/BA and HS4/DO8 transitions.

**Figure 4.** Spline fits to combined ice core data and calculated source changes for the Heinrich Stadial 4/Dansgaard Oeschger 8 transition. The uncertainty bands represent  $2\sigma$  of the full ensemble of spline fits to the data and  $1\sigma$  of the calculated source changes. Gray bands with diagonal lines show the expected deltas and  $1\sigma$  uncertainty assuming that the fraction of emissions does not change. Gray bands with vertical lines demonstrate the expected  $\Delta E_{nit}^*$  and  $\Delta E_{den}$  emissions changes for a “null hypothesis” in which nitrification remained the dominant pathway in the ocean and denitrification remained dominant on land. Dashed red lines show the results if the range in end member isotopic values is adjusted  $+15\text{‰}$  for 92% reduction of  $N_2O$  produced by denitrification.

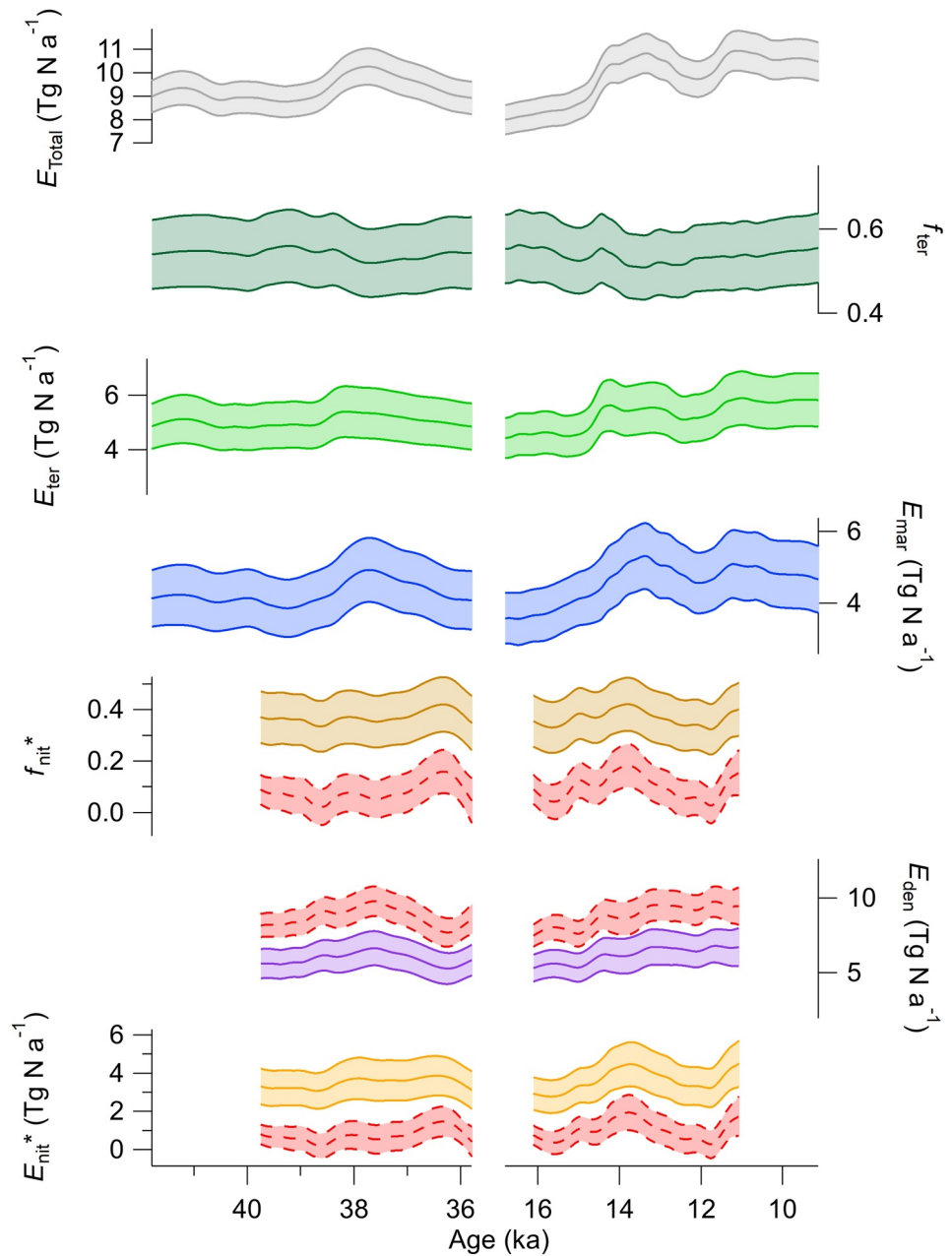


**Figure 5.** Absolute emissions and source fractions ( $f_{\text{nit}}^*$  and  $f_{\text{ter}}$ ) from the model—land versus ocean, and nitrification (with possible contribution from fungal denitrification) versus denitrification - for both time periods. The uncertainty bands represent 1-sigma of the full ensemble of solutions. The red lines represent average and 1-sigma ensembles assuming 92% reduction of the  $\text{N}_2\text{O}$  pool produced by denitrification and resultant shift in  $\delta^{15}\text{N}^{\text{SP}}$  of the denitrification end member value (Table 1).

We compare our reconstructions to Pa/Th ratios measured in Bermuda Rise sediments (Figure 6), a well-established proxy for the strength of the AMOC. Rapid changes in AMOC drove the transitions from stadial to interstadial conditions, for example, at HS4/DO8 and HS1/BA, and reinvigorated the shallow marine nitrogen cycle by redistributing nutrients to shallow surface and thermocline waters (Schmittner & Galbraith, 2008). The enhanced circulation may have also vented  $\text{N}_2\text{O}$  produced in the deep ocean when AMOC was sluggish. These transitions also manifested on land via atmospheric “teleconnections,” essentially redistributions of heat between the hemispheres, that controlled  $\text{N}_2\text{O}$  emissions by increasing/decreasing soil temperatures and shifting the tropical rain belts to increase/decrease soil moisture content (Rhodes et al., 2015). AMOC resummptions are

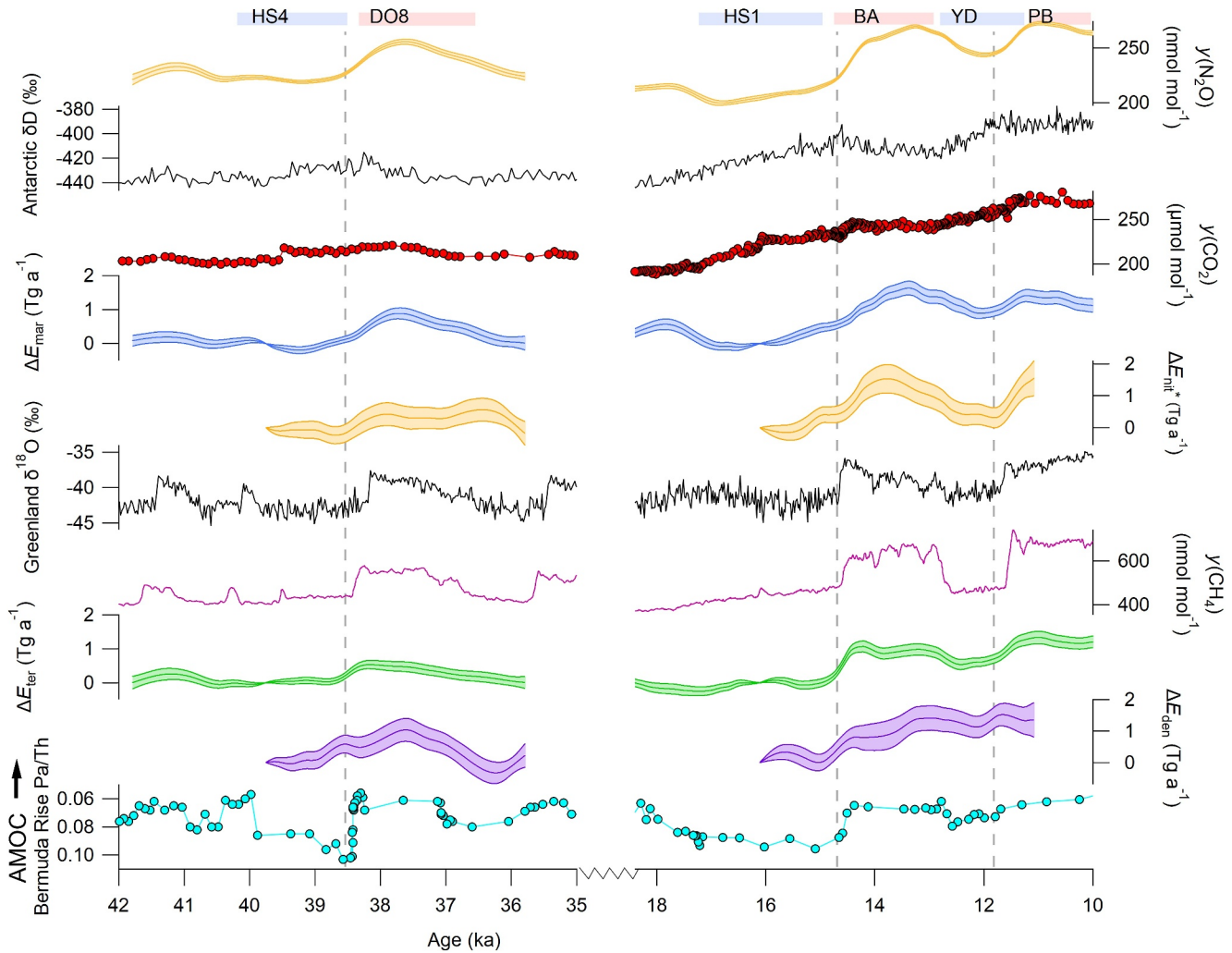


**Figure 6.**  $\text{N}_2\text{O}$  reconstructions from the Heinrich Stadial 4/Dansgaard Oeschger 8 transition compared to the last deglaciation, as well as Antarctic (Dome C) temperature (ice  $\delta\text{D}$ ),  $\text{CO}_2$ , Greenland (NGRIP) temperature ( $\delta^{18}\text{O}$ ),  $\text{CH}_4$ , and Pa/Th proxy records for AMOC strength. Note the discontinuous time axis. Data citations (Andersen et al., 2004; Bauska et al., 2021; Henry et al., 2016; Jouzel et al., 2007; McManus et al., 2004; Rhodes et al., 2015).

characterized by rapid Northern Hemisphere warming, reflected in the sharp increases in Greenland  $\delta^{18}\text{O}$  at the DO8, BA, and PB, and rapid acceleration of  $\text{N}_2\text{O}$  emissions from land sources, mirrored by sharp increases in  $\text{CH}_4$ , with slightly delayed (but accelerating) emissions from marine sources (Figure 6). The reconstructions of  $\text{N}_2\text{O}$  emissions from our two end members—nitrification (with possible contribution from fungal denitrification) and denitrification pathways—show that AMOC resumption triggered an increase in  $\text{N}_2\text{O}$  from both production pathways at each of the three instances in our records (Figure 6). We tentatively observe nuanced differences in the exact response of  $\text{N}_2\text{O}$  emissions from nitrification and denitrification to AMOC changes. For one, nitrification generally increases rapidly immediately following AMOC restarts and continues to increase for the next half millennium, broadly in phase with marine  $\text{N}_2\text{O}$  emission changes (Figure 6). Denitrification-sourced  $\text{N}_2\text{O}$ , on the other hand, accelerates sharply in phase with land emissions at the HS1/BA transition, which is expected if  $\text{N}_2\text{O}$  from terrestrial environments is predominantly produced by denitrification, but during the HS4/DO8 or the YD/PB transitions the denitrification source seems to be flattening as land emissions accelerate. These features are not robust when considering the uncertainties in the model results, but nevertheless we highlight them as a matter for future study. A more striking difference revealed in our reconstructions is that the  $\text{N}_2\text{O}$  decrease during the YD (and recovery into the PB) was almost wholly driven by nitrification (with possible fungal denitrification) changes, whereas the decrease in  $\text{N}_2\text{O}$  following the DO8 warming was predominantly due to a waning denitrification source (with nitrification source sustaining through most of the  $\text{N}_2\text{O}$  decline) (Figure 6). We have

already highlighted the dependence of this result on a low number of data points, but if proven to be a robust feature by future analyses, this could point to a different balance of nitrification and denitrification in marine and terrestrial environments during the YD versus DO8, perhaps implicating a role for denitrification during AMOC events of the last ice age.

A major caveat in our assertions is that the contribution from fungal denitrification to total  $N_2O$  emissions is severely underconstrained by  $N_2O$  isotopes. The reason is that there is overlap in the  $\delta^{15}N^{SP}$  signatures of  $N_2O$  from fungal denitrification and nitrifying bacteria. There is also overlap between  $\delta^{18}O$  for fungal denitrification and marine emissions, precluding the disentanglement of fungal denitrification from nitrification end members by way of using  $\delta^{18}O$ . As such, our estimates of marine versus terrestrial emissions could also be biased if the fungal denitrification contribution to total  $N_2O$  emissions were significant. Until this is constrained with independent methods, or it is shown that the isotopic signature of fungal denitrification is in fact distinct, we can only assert that we have produced a reasonable and plausible estimate of global  $N_2O$  emissions sources.

We conclude our discussion by pointing out that the work presented here does not rule out a scenario that can broadly be considered a “null hypothesis,” that is, where all sources of  $N_2O$  (marine, terrestrial, nitrification, denitrification) played an important role in increasing atmospheric  $N_2O$  during global warming events of the past, and where nitrification and denitrification remained the dominant production pathways in the marine and terrestrial environments, respectively.

## 5. Conclusions

New ice core measurements of position-specific  $N_2O$  isotopic composition offer powerful constraints for probing the causes of atmospheric  $N_2O$  changes in the past. The data illustrate that the abrupt rise in  $N_2O$  across the last deglaciation was plausibly driven by increased emissions of  $N_2O$  from both nitrification and denitrification. Similar measurements across an abrupt, smaller magnitude rise in  $N_2O$  during the last ice age implicate nitrification and denitrification pathways, while demonstrating for the first time the relative  $N_2O$  contribution from land and marine sources for one of these events. The data and analyses present a clear picture of increasing  $N_2O$  emissions from both microbial pathways in response to warming, likely in association with shifts in the strength of the Atlantic Meridional Overturning Circulation. AMOC changes appear to affect marine and terrestrial  $N_2O$  production similarly in three separate instances. Within our data and model uncertainties, we conclude that both pathways play an important role in driving past  $N_2O$  changes, and we do not reject a “null hypothesis” scenario in which nitrification and denitrification remained the dominant  $N_2O$  production pathways in the oceans and on land, respectively.

The interpretations in this study hinge on the values of  $N_2O$  source isotopic signatures as well as the trends resolved in ice core data. Systematic uncertainties in the source signatures may exist that are related to the degree of  $N_2O$  reduction and contributions from fungal denitrification that cannot be quantified by existing data. Reducing the uncertainty in source signatures, analytical precision, and time-resolution gaps will increase the power of the ice core  $N_2O$  isotope records. We optimistically look forward to these improvements, which will inevitably provide more clarity on the causes of  $N_2O$  variations during the last ice age and improve our ability to model  $N_2O$ -climate feedback that are important for predicting the future trajectory of this greenhouse gas in a warming world. Future work should focus on (a) whether the site preference distinction is robust in natural  $N_2O$  producing ecosystems or the complications are too great to be of use for reliably deconvolving the  $N_2O$  production pathways in ice cores, and (b) utilizing  $\delta^{18}O$  in  $N_2O$  source reconstructions, including to constrain the degree of  $N_2O$  reduction in denitrifying environments.

## Conflict of Interest

The authors declare no conflicts of interest relevant to this study.

## Data Availability Statement

Data are publicly available at the United States Antarctic Program data repository Menking and Brook (2025) (USAP-DC, <https://www.usap-dc.org/view/project/p0010465>). Other data on which this article is based are available in Fischer et al. (2019), Schilt et al. (2014).

**Acknowledgments**

We thank T. Bauska (British Antarctic Survey) and S. Shackleton (Massachusetts Institute of Technology) for diligent sampling at the Taylor Glacier main transect, and we thank S. Toyoda and N. Yoshida (TiTech) and J. Mohn (EMPA) for N<sub>2</sub>O isotopic calibration gases. The University of Bern gratefully acknowledges financial support by the Swiss National Science Foundation (Award 172506 and 200328). Oregon State University gratefully acknowledges financial support from the National Science Foundation (Award 1903681). Open access publishing facilitated by University of Tasmania, as part of the Wiley - University of Tasmania agreement via the Council of Australian University Librarians.

**References**

Aciego, S. M., Cuffey, K. M., Kavanaugh, J. L., Morse, D. L., & Severinghaus, J. P. (2007). Pleistocene ice and paleo-strain rates at Taylor Glacier, Antarctica. *Quaternary Research*, 68(3), 303–313. <https://doi.org/10.1016/j.yqres.2007.07.013>

Altabet, M. A., Higginson, M. J., & Murray, D. W. (2002). The effect of millennial-scale changes in Arabian Sea denitrification on atmospheric CO<sub>2</sub>. *Nature*, 415(6868), 159–162. <https://doi.org/10.1038/415159a>

Andersen, K. K., Azuma, N., Barnola, J. M., Bigler, M., Biscaye, P., Cailion, N., et al. (2004). High-resolution record of Northern Hemisphere climate extending into the last interglacial period. *Nature*, 431(7005), 147–151. <https://doi.org/10.1038/nature02805>

Baggenstos, D., Bauska, T. K., Severinghaus, J. P., Lee, J. E., Schaefer, H., Buizert, C., et al. (2017). Atmospheric gas records from Taylor Glacier, Antarctica, reveal ancient ice with ages spanning the entire last glacial cycle. *Climate of the Past*, 13(7), 943–958. <https://doi.org/10.5194/cp-13-943-2017>

Baggenstos, D., Severinghaus, J. P., Mulvaney, R., McConnell, J. R., Sigl, M., Maselli, O., et al. (2018). A horizontal ice core from Taylor Glacier, its implications for Antarctic climate history, and an improved Taylor Dome ice core time scale. *Paleoceanography and Paleoclimatology*, 33(7), 778–794. <https://doi.org/10.1029/2017pa003297>

Bange, H. W., Rapsomanikis, S., & Andreae, M. O. (2001). Nitrous oxide cycling in the Arabian sea. *Journal of Geophysical Research*, 106(C1), 1053–1065. <https://doi.org/10.1029/1999jc000284>

Battaglia, G., & Joos, F. (2018). Marine N<sub>2</sub>O emissions from nitrification and denitrification constrained by modern observations and projected in Multimillennial global warming simulations. *Global Biogeochemical Cycles*, 32(1), 92–121. <https://doi.org/10.1002/2017gb005671>

Bauska, T. K., Baggenstos, D., Brook, E. J., Mix, A. C., Marcott, S. A., Petrenko, V. V., et al. (2016). Carbon isotopes characterize rapid changes in atmospheric carbon dioxide during the last deglaciation. *Proceedings of the National Academy of Sciences of the United States of America*, 113(13), 3465–3470. <https://doi.org/10.1073/pnas.1513868113>

Bauska, T. K., Brook, E. J., Marcott, S. A., Baggenstos, D., Shackleton, S., Severinghaus, J. P., & Petrenko, V. V. (2018). Controls on millennial-scale atmospheric CO<sub>2</sub> variability during the last glacial period. *Geophysical Research Letters*, 45(15), 7731–7740. <https://doi.org/10.1029/2018gl077881>

Bauska, T. K., Marcott, S. A., & Brook, E. J. (2021). Abrupt changes in the global carbon cycle during the last glacial period. *Nature Geoscience*, 14(2), 18–96. <https://doi.org/10.1038/s41561-020-00680-2>

Bernard, S., Rockmann, T. R., Kaiser, J., Barnola, J. M., Fischer, H., Blunier, T., & Chappellaz, J. (2006). Constraints on N<sub>2</sub>O budget changes since pre-industrial time from new firn air and ice core isotope measurements. *Atmospheric Chemistry and Physics*, 6(2), 493–503. <https://doi.org/10.5194/acp-6-493-2006>

Bösch, Y., Pold, G., Saghai, A., Karlsson, M., Jones, C. M., & Hallin, S. (2023). Distribution and environmental drivers of fungal denitrifiers in global soils. *Microbiology Spectrum*, 11(3), 14. <https://doi.org/10.1128/spectrum.00061-23>

Bouwman, A. F., Beusen, A. H. W., Griffioen, J., Van Groenigen, J. W., Hefting, M. M., Oenema, O., et al. (2013). Global trends and uncertainties in terrestrial denitrification and N<sub>2</sub>O emissions. *Philosophical Transactions of the Royal Society B: Biological Sciences*, 368(1621), 11. <https://doi.org/10.1098/rstb.2013.0112>

Bouwman, A. F., Fung, I., Matthews, E., & John, J. (1993). Global analysis of the potential for N<sub>2</sub>O production in natural soils. *Global Biogeochemical Cycles*, 7(3), 557–597. <https://doi.org/10.1029/93gb01186>

Buchen, C., Lewicka-Szczebak, D., Flessa, H., & Well, R. (2018). Estimating N<sub>2</sub>O processes during grassland renewal and grassland conversion to maize cropping using N<sub>2</sub>O isotopocules. *Rapid Communications in Mass Spectrometry*, 32(13), 1053–1067. <https://doi.org/10.1002/rcm.8132>

Buizert, C., Adrian, B., Ahn, J., Albert, M., Alley, R. B., Baggenstos, D., et al. (2015). Precise inter-polar phasing of abrupt climate change during the last ice age. *Nature*, 520(7549), 661–665. <https://doi.org/10.1038/nature14401>

Buizert, C., Baggenstos, D., Jiang, W., Purtschert, R., Petrenko, V. V., Lu, Z. T., et al. (2014). Radiometric Kr-81 dating identifies 120,000-year-old ice at Taylor Glacier, Antarctica. *Proceedings of the National Academy of Sciences of the United States of America*, 111(19), 6876–6881. <https://doi.org/10.1073/pnas.1320329111>

Buizert, C., Cuffey, K. M., Severinghaus, J. P., Baggenstos, D., Fudge, T. J., Steig, E. J., et al. (2015). The WAIS Divide deep ice core WD2014 chronology - Part I: Methane synchronization (68–31 kaBP) and the gas age-ice age difference. *Climate of the Past*, 11(2), 153–173. <https://doi.org/10.5194/cp-11-153-2015>

Buizert, C., Sigl, M., Severi, M., Markle, B. R., Wettstein, J. J., McConnell, J. R., et al. (2018). Abrupt ice-age shifts in southern westerly winds and Antarctic climate forced from the north. *Nature*, 563(7733), 681–685. <https://doi.org/10.1038/s41586-018-0727-5>

Butterbach-Bahl, K., Baggs, E. M., Dannenmann, M., Kiese, R., & Zechmeister-Boltenstern, S. (2013). Nitrous oxide emissions from soils: How well do we understand the processes and their controls? *Philosophical Transactions of the Royal Society B: Biological Sciences*, 368(1621), 20130122. <https://doi.org/10.1098/rstb.2013.0122>

Ciais, P., Sabine, C., Bala, G., Bopp, L., Brovkin, V., Canadell, J. G., et al. (2013). Carbon and other biogeochemical cycles (climate change 2013): The physical science basis. *Contribution of Working Group 1 to the Fifth Assessment Report of the Intergovernmental on Climate Change, Issue*.

Cliff, E., Khaliwala, S., & Schmittner, A. (2021). Glacial deep ocean deoxygenation driven by biologically mediated air-sea disequilibrium. *Nature Geoscience*, 14(1), 43–50. <https://doi.org/10.1038/s41561-020-00667-z>

Denk, T. R. A., Mohn, J., Decock, C., Lewicka-Szczebak, D., Harris, E., Butterbach-Bahl, K., et al. (2017). The nitrogen cycle: A review of isotope effects and isotope modeling approaches. *Soil Biology and Biochemistry*, 105, 121–137. <https://doi.org/10.1016/j.soilbio.2016.11.015>

Dore, J. E., Popp, B. N., Karl, D. M., & Sansone, F. J. (1998). A large source of atmospheric nitrous oxide from subtropical North Pacific surface waters. *Nature*, 396(6706), 63–66. <https://doi.org/10.1038/23921>

Dyonisius, M. N., Petrenko, V. V., Smith, A. M., Hua, Q., Yang, B., Schmitt, J., et al. (2020). Old carbon reservoirs were not important in the deglacial methane budget. *Science*, 367(6480), 907–910. <https://doi.org/10.1126/science.aax0504>

Eggleston, S., Schmitt, J., Bereiter, B., Schneider, R., & Fischer, H. (2016). Evolution of the stable carbon isotope composition of atmospheric CO<sub>2</sub> over the last glacial cycle. *Paleoceanography*, 31(3), 434–452. <https://doi.org/10.1002/2015pa002874>

Enting, I. G. (1987). On the use of smoothing splines to filter CO<sub>2</sub> data. *Journal of Geophysical Research*, 92(D9), 10977–10984. <https://doi.org/10.1029/JD092iD09p10977>

Etheridge, D. M., Steele, L. P., Langenfelds, R. L., Francey, R. J., Barnola, J. M., & Morgan, V. I. (1996). Natural and anthropogenic changes in atmospheric CO<sub>2</sub> over the last 1000 years from air in Antarctic ice and firn. *Journal of Geophysical Research*, 101(D2), 4115–4128. <https://doi.org/10.1029/95jd03410>

- Farias, L., Castro-Gonzalez, M., Cornejo, M., Charpentier, J., Faundez, J., Boontan, N., & Yoshida, N. (2009). Denitrification and nitrous oxide cycling within the upper oxycline of the eastern tropical South Pacific oxygen minimum zone. *Limnology & Oceanography*, *54*(1), 132–144. <https://doi.org/10.4319/lo.2009.54.1.0132>
- Fischer, H., Schmitt, J., Bock, M., Seth, B., Joos, F., Spahni, R., et al. (2019). N<sub>2</sub>O changes from the Last Glacial Maximum to the preindustrial - Part 1: Quantitative reconstruction of terrestrial and marine emissions using N<sub>2</sub>O stable isotopes in ice cores. *Biogeosciences*, *16*(20), 3997–4021. <https://doi.org/10.5194/bg-16-3997-2019>
- Flückiger, J., Blunier, T., Stauffer, B., Chappellaz, J., Spahni, R., Kawamura, K., et al. (2004). N<sub>2</sub>O and CH<sub>4</sub> variations during the last glacial epoch: Insight into global processes. *Global Biogeochemical Cycles*, *18*(1), Gb1020. <https://doi.org/10.1029/2003gb002122>
- Flückiger, J., Dallenbach, A., Blunier, T., Stauffer, B., Stocker, T. F., Raynaud, D., & Barnola, J. M. (1999). Variations in atmospheric N<sub>2</sub>O concentration during abrupt climatic changes. *Science*, *285*(5425), 227–230. <https://doi.org/10.1126/science.285.5425.227>
- Frame, C. H., Deal, E., Nevison, C. D., & Casciotti, K. L. (2014). N<sub>2</sub>O production in the eastern South Atlantic: Analysis of N<sub>2</sub>O stable isotopic and concentration data. *Global Biogeochemical Cycles*, *28*(11), 1262–1278. <https://doi.org/10.1002/2013gb004790>
- Freitag, A., Wallace, D. W. R., & Bange, H. W. (2012). Global oceanic production of nitrous oxide. *Philosophical Transactions of the Royal Society B: Biological Sciences*, *367*(1593), 1245–1255. <https://doi.org/10.1098/rstb.2011.0360>
- Galbraith, E. D., Kienast, M., Albuquerque, A. L., Altabet, M. A., Batista, F., Bianchi, D., et al. (2013). The acceleration of oceanic denitrification during deglacial warming. *Nature Geoscience*, *6*(7), 579–584. <https://doi.org/10.1038/ngeo1832>
- Ganeshram, R. S., Pedersen, T. F., Calvert, S. E., McNeill, G. W., & Fontugne, M. R. (2000). Glacial-interglacial variability in denitrification in the world's oceans: Causes and consequences. *Paleoceanography*, *15*(4), 361–376. <https://doi.org/10.1029/1999pa000422>
- Ghosh, S., Toyoda, S., Buiertz, C., Etheridge, D., Langenfelds, R., Yoshida, N., et al. (2023). Concentration and isotopic composition of atmospheric N<sub>2</sub>O over the last century. *Journal of Geophysical Research: Atmospheres*, *128*(12), 1–18. <https://doi.org/10.1029/2022JD038281>
- Hall, B. D., Dutton, G. S., & Elkins, J. W. (2007). The NOAA nitrous oxide standard scale for atmospheric observations. *Journal of Geophysical Research*, *112*(D9), D09305. <https://doi.org/10.1029/2006jd007954>
- Henry, L. G., McManus, J. F., Curry, W. B., Roberts, N. L., Piotrowski, A. M., & Keigwin, L. D. (2016). North Atlantic ocean circulation and abrupt climate change during the last glaciation. *Science*, *353*(6298), 470–474. <https://doi.org/10.1126/science.aaf5529>
- Ishijima, K., Sugawara, S., Kawamura, K., Hashida, G., Morimoto, S., Murayama, S., et al. (2007). Temporal variations of the atmospheric nitrous oxide concentration and its delta N-15 and delta O-18 for the latter half of the 20th century reconstructed from firn air analyses. *Journal of Geophysical Research*, *112*(D3), D03305. <https://doi.org/10.1029/2006jd007208>
- Jaccard, S., Galbraith, E., Frölicher, T., & Gruber, N. (2014). Ocean (De)oxygenation across the last deglaciation: Insights for the future. *Oceanography*, *27*(1), 26–35. <https://doi.org/10.5670/oceanog.2014.05>
- Jaccard, S. L., & Galbraith, E. D. (2012). Large climate-driven changes of oceanic oxygen concentrations during the last deglaciation. *Nature Geoscience*, *5*(2), 151–156. <https://doi.org/10.1038/ngeo1352>
- Joos, F., Battaglia, G., Fischer, H., Jeltsch-Thommes, A., & Schmitt, J. (2019). Marine N<sub>2</sub>O emissions during a Younger Dryas-like event: The role of meridional overturning, tropical thermocline ventilation, and biological productivity. *Environmental Research Letters*, *14*(7), 075007. <https://doi.org/10.1088/1748-9326/ab2353>
- Jouzel, J., Masson-Delmotte, V., Cattani, O., Dreyfus, G., Falourd, S., Hoffmann, G., et al. (2007). Orbital and millennial Antarctic climate variability over the past 800,000 years. *Science*, *317*(5839), 793–796. <https://doi.org/10.1126/science.1141038>
- Kaiser, J., Park, S., Boering, K. A., Brenninkmeijer, C. A. M., Hilkert, A., & Rockmann, T. (2004). Mass spectrometric method for the absolute calibration of the intramolecular nitrogen isotope distribution in nitrous oxide. *Analytical and Bioanalytical Chemistry*, *378*(2), 256–269. <https://doi.org/10.1007/s00216-003-2233-2>
- Kaiser, J., & Röckmann, T. (2008). Correction of mass spectrometric isotope ratio measurements for isobaric isotopologues of O-2, CO, CO<sub>2</sub>, N<sub>2</sub>O and SO<sub>2</sub>. *Rapid Communications in Mass Spectrometry*, *22*(24), 3997–4008. <https://doi.org/10.1002/rcm.3821>
- Kavanaugh, J. L., & Cuffey, K. M. (2009). Dynamics and mass balance of Taylor Glacier, Antarctica: 2. Force balance and longitudinal coupling. *Journal of Geophysical Research*, *114*(11), F04011. <https://doi.org/10.1029/2009jf001329>
- Kavanaugh, J. L., Cuffey, K. M., Morse, D. L., Conway, H., & Rignot, E. (2009). Dynamics and mass balance of Taylor Glacier, Antarctica: 1. Geometry and surface velocities. *Journal of Geophysical Research*, *114*(F4), F04010. <https://doi.org/10.1029/2009jf001309>
- Kelly, C. L., Manning, C., Frey, C., Kaiser, J., Gluschkoff, N., & Casciotti, K. L. (2023). Pysisotopomer: A Python package for obtaining intramolecular isotope ratio differences from mass spectrometric analysis of nitrous oxide isotopocules. *Rapid Communications in Mass Spectrometry*, *37*(11), 17. <https://doi.org/10.1002/rcm.9513>
- Kim, K. R., & Craig, H. (1993). N-15 and O-18 characteristics of nitrous oxide - a global perspective. *Science*, *262*(5141), 1855–1857. <https://doi.org/10.1126/science.262.5141.1855>
- Laughlin, R. J., & Stevens, R. J. (2002). Evidence for fungal dominance of denitrification and codenitrification in a grassland soil. *Soil Science Society of America Journal*, *66*(5), 1540–1548. <https://doi.org/10.2136/sssaj2002.1540>
- Lewicka-Szczębak, D., Lewicki, M., & Well, R. (2020). N<sub>2</sub>O isotope approaches for source partitioning of N<sub>2</sub>O production and estimation of N<sub>2</sub>O reduction - Validation with the <sup>15</sup>N gas-flux method in laboratory and field studies. *Biogeosciences*, *17*(22), 5513–5537. <https://doi.org/10.5194/bg-17-5513-2020>
- Lewicka-Szczębak, D., Well, R., Koster, J. R., Fuss, R., Senbayram, M., Dittler, K., & Flessa, H. (2014). Experimental determinations of isotopic fractionation factors associated with N<sub>2</sub>O production and reduction during denitrification in soils. *Geochimica et Cosmochimica Acta*, *134*, 55–73. <https://doi.org/10.1016/j.gca.2014.03.010>
- McManus, J. F., Francois, R., Gherardi, J. M., Keigwin, L. D., & Brown-Leger, S. (2004). Collapse and rapid resumption of Atlantic meridional circulation linked to deglacial climate changes. *Nature*, *428*(6985), 834–837. <https://doi.org/10.1038/nature02494>
- Menking, J. A., & Brook, E. J. (2025). Deciphering changes in atmospheric nitrous oxide concentration during the last ice age using the intramolecular site-preference of nitrogen isotopes [Dataset]. *United States Antarctic Program Data Center*. <https://www.usap-dc.org/view/project/p0010465>
- Menking, J. A., Brook, E. J., Schilt, A., Shackleton, S., Dyonisius, M., Severinghaus, J. P., & Petrenko, V. V. (2020). Millennial-scale changes in terrestrial and marine nitrous oxide emissions at the onset and termination of marine isotope stage 4. *Geophysical Research Letters*, *47*(22), e2020GL089110. <https://doi.org/10.1029/2020gl089110>
- Menking, J. A., Brook, E. J., Shackleton, S. A., Severinghaus, J. P., Dyonisius, M. N., Petrenko, V., et al. (2019). Spatial pattern of accumulation at Taylor Dome during marine isotope stage 4: Stratigraphic constraints from Taylor Glacier. *Climate of the Past*, *15*(4), 1537–1556. <https://doi.org/10.5194/cp-15-1537-2019>
- Menking, J. A., Shackleton, S. A., Bauska, T. K., Buffen, A. M., Brook, E. J., Barker, S., et al. (2022). Multiple carbon cycle mechanisms associated with the glaciation of Marine Isotope Stage 4. *Nature Communications*, *13*(1), 5443. <https://doi.org/10.1038/s41467-022-33166-3>

- Miteva, V., Sowers, T., Schupbach, S., Fischer, H., & Brenchley, J. (2016). Geochemical and microbiological studies of nitrous oxide variations within the new NEEM Greenland ice core during the last glacial period. *Geomicrobiology Journal*, 33(8), 647–660. <https://doi.org/10.1080/01490451.2015.1074321>
- Moffitt, S. E., Moffitt, R. A., Sauthoff, W., Davis, C. V., Hewett, K., & Hill, T. M. (2015). Paleooceanographic insights on recent oxygen minimum zone expansion: Lessons for modern oceanography. *PLoS One*, 10(1), e0115246. <https://doi.org/10.1371/journal.pone.0115246>
- Naqvi, S. W. A., Bange, H. W., Farias, L., Monteiro, P. M. S., Scranton, M. I., & Zhang, J. (2010). Marine hypoxia/anoxia as a source of CH<sub>4</sub> and N<sub>2</sub>O. *Biogeosciences*, 7(7), 2159–2190. <https://doi.org/10.5194/bg-7-2159-2010>
- Nevison, C., Butler, J. H., & Elkins, J. W. (2003). Global distribution of N<sub>2</sub>O and the Delta N<sub>2</sub>O-AOU yield in the subsurface ocean. *Global Biogeochemical Cycles*, 17(4), 1119. <https://doi.org/10.1029/2003gb002068>
- Ostrom, N. E., Pitt, A., Sutka, R., Ostrom, P. H., Grandy, A. S., Huizinga, K. M., & Robertson, G. P. (2007). Isotopologue effects during N<sub>2</sub>O reduction in soils and in pure cultures of denitrifiers. *Journal of Geophysical Research*, 112(G2), G02005. <https://doi.org/10.1029/2006jg000287>
- Park, S., Croteau, P., Boering, K. A., Etheridge, D. M., Ferretti, D., Fraser, P. J., et al. (2012). Trends and seasonal cycles in the isotopic composition of nitrous oxide since 1940. *Nature Geoscience*, 5(4), 261–265. <https://doi.org/10.1038/ngeo1421>
- Park, S., Perez, T., Boering, K. A., Trumbore, S. E., Gil, J., Marquina, S., & Tyler, S. C. (2011). Can N<sub>2</sub>O stable isotopes and isotopomers be useful tools to characterize sources and microbial pathways of N<sub>2</sub>O production and consumption in tropical soils? *Global Biogeochemical Cycles*, 25(16), Gb1001. <https://doi.org/10.1029/2009gb003615>
- Petrenko, V. V., Mith, A. M. S., Chaefer, H. S., Riedel, K., Brook, E., Baggenstos, D., et al. (2017). Minimal geological methane emissions during the Younger Dryas-Preboreal abrupt warming event. *Nature*, 548(7668), 443–446. <https://doi.org/10.1038/nature23316>
- Popp, B. N., Westley, M. B., Toyoda, S., Miwa, T., Dore, J. E., Yoshida, N., et al. (2002). Nitrogen and oxygen isotopomeric constraints on the origins and sea-to-air flux of N<sub>2</sub>O in the oligotrophic subtropical North Pacific gyre. *Global Biogeochemical Cycles*, 16(4), 1064. <https://doi.org/10.1029/2001gb001806>
- Prather, M. J., Hsu, J., DeLuca, N. M., Jackman, C. H., Oman, L. D., Douglass, A. R., et al. (2015). Measuring and modeling the lifetime of nitrous oxide including its variability. *Journal of Geophysical Research-Atmospheres*, 120(11), 5693–5705. <https://doi.org/10.1002/2015jd023267>
- Prokopiou, M., Martinier, P., Sapart, C. J., Witrant, E., Monteil, G., Ishijima, K., et al. (2017). Constraining N<sub>2</sub>O emissions since 1940 using firn air isotope measurements in both hemispheres. *Atmospheric Chemistry and Physics*, 17(7), 4539–4564. <https://doi.org/10.5194/acp-17-4539-2017>
- Prokopiou, M., Sapart, C. J., Rosen, J., Sperlich, P., Blunier, T., Brook, E., et al. (2018). Changes in the isotopic signature of atmospheric nitrous oxide and its global average source during the last three millennia. *Journal of Geophysical Research: Atmospheres*, 123(18), 10757–10773. <https://doi.org/10.1029/2018JD029008>
- Ravishankara, A. R., Daniel, J. S., & Portmann, R. W. (2009). Nitrous oxide (N<sub>2</sub>O): The dominant ozone-depleting substance emitted in the 21st century. *Science*, 326(5949), 123–125. <https://doi.org/10.1126/science.1176985>
- Rhodes, R. H., Brook, E. J., Chiang, J. C. H., Blunier, T., Maselli, O. J., McConnell, J. R., et al. (2015). Enhanced tropical methane production in response to iceberg discharge in the North Atlantic. *Science*, 348(6238), 1016–1019. <https://doi.org/10.1126/science.1262005>
- Röckmann, T., Kaiser, J., & Brenninkmeijer, C. A. M. (2003). The isotopic fingerprint of the pre-industrial and the anthropogenic N<sub>2</sub>O source. *Atmospheric Chemistry and Physics*, 3(2), 315–323. <https://doi.org/10.5194/acp-3-315-2003>
- Röckmann, T., Kaiser, J., Brenninkmeijer, C. A. M., Crowley, J. N., Borchers, R., Brand, W. A., & Crutzen, P. J. (2001). Isotopic enrichment of nitrous oxide ((NNO)-N-15-N-14, (NNO)-N-14-N-15, (NNO)-N-14-N-14-O-18) in the stratosphere and in the laboratory. *Journal of Geophysical Research*, 106(D10), 10403–10410. <https://doi.org/10.1029/2000jd900822>
- Rohe, L., Anderson, T. H., Flessa, H., Goeske, A., Lewicka-Szczepak, D., Wrage-Mönnig, N., & Well, R. (2021). Comparing modified substrate-induced respiration with selective inhibition (SIRIN) and N<sub>2</sub>O isotope approaches to estimate fungal contribution to denitrification in three arable soils under anoxic conditions. *Biogeosciences*, 18(15), 4629–4650. <https://doi.org/10.5194/bg-18-4629-2021>
- Scheer, C., Fuchs, K., Pelster, D., & Butterbach-Bahl, K. (2020). Estimating global terrestrial denitrification from measured N<sub>2</sub>O: (N<sub>2</sub>O + N<sub>2</sub>) product ratios. *Current Opinion in Environmental Sustainability*, 47, 72–80. <https://doi.org/10.1016/j.cosust.2020.07.005>
- Schilt, A., Baumgartner, M., Blunier, T., Schwander, J., Spahni, R., Fischer, H., & Stocker, T. F. (2010). Glacial-interglacial and millennial-scale variations in the atmospheric nitrous oxide concentration during the last 800,000 years. *Quaternary Science Reviews*, 29(1–2), 182–192. <https://doi.org/10.1016/j.quascirev.2009.03.011>
- Schilt, A., Baumgartner, M., Eicher, O., Chappellaz, J., Schwander, J., Fischer, H., & Stocker, T. F. (2013). The response of atmospheric nitrous oxide to climate variations during the last glacial period. *Geophysical Research Letters*, 40(9), 1888–1893. <https://doi.org/10.1002/grl.50380>
- Schilt, A., Baumgartner, M., Schwander, J., Buiron, D., Capron, E., Chappellaz, J., et al. (2010). Atmospheric nitrous oxide during the last 140,000 years. *Earth and Planetary Science Letters*, 300(1–2), 33–43. <https://doi.org/10.1016/j.epsl.2010.09.027>
- Schilt, A., Brook, E. J., Bauska, T. K., Baggenstos, D., Fischer, H., Joos, F., et al. (2014). Isotopic constraints on marine and terrestrial N<sub>2</sub>O emissions during the last deglaciation. *Nature*, 516(7530), 234–237. <https://doi.org/10.1038/nature13971>
- Schmitt, J., Seth, B., Bock, M., & Fischer, H. (2014). Online technique for isotope and mixing ratios of CH<sub>4</sub>, N<sub>2</sub>O, Xe and mixing ratios of organic trace gases on a single ice core sample. *Atmospheric Measurement Techniques*, 7(8), 2645–2665. <https://doi.org/10.5194/amt-7-2645-2014>
- Schmittner, A., & Galbraith, E. D. (2008). Glacial greenhouse-gas fluctuations controlled by ocean circulation changes. *Nature*, 456(7220), 373–376. <https://doi.org/10.1038/nature07531>
- Schmittner, A., Galbraith, E. D., Hostetler, S. W., Pedersen, T. F., & Zhang, R. (2007). Large fluctuations of dissolved oxygen in the Indian and Pacific oceans during Dansgaard-Oeschger oscillations caused by variations of North Atlantic Deep Water subduction. *Paleoceanography*, 22(3), Pa3207. <https://doi.org/10.1029/2006pa001384>
- Shackleton, S., Baggenstos, D., Menking, J. A., Dyonisius, M. N., Bereiter, B., Bauska, T. K., et al. (2020). Global ocean heat content in the Last Interglacial. *Nature Geoscience*, 13(1), 7–81. <https://doi.org/10.1038/s41561-019-0498-0>
- Shackleton, S., Menking, J. A., Brook, E., Buizert, C., Dyonisius, M., Petrenko, V., et al. (2021). Evolution of mean ocean temperature in marine isotope stage 4. *Climate of the Past*, 17(5), 2273–2289. <https://doi.org/10.5194/cp-17-2273-2021>
- Snider, D. M., Venkiteswaran, J. J., Schiff, S. L., & Spoelstra, J. (2015). From the ground up: Global nitrous oxide sources are constrained by stable isotope values. *PLoS One*, 10(3), e0118954. <https://doi.org/10.1371/journal.pone.0118954>
- Sowers, T. (2001). N<sub>2</sub>O record spanning the penultimate deglaciation from the Vostok ice core. *Journal of Geophysical Research*, 106(D23), 31903–31914. <https://doi.org/10.1029/2000jd900707>
- Sowers, T., Alley, R. B., & Jubenville, J. (2003). Ice core records of atmospheric N<sub>2</sub>O covering the last 106,000 years. *Science*, 301(5635), 945–948. <https://doi.org/10.1126/science.1085293>

- Sowers, T., Rodebaugh, A., Yoshida, N., & Toyoda, S. (2002). Extending records of the isotopic composition of atmospheric N<sub>2</sub>O back to 1800 AD from air trapped in snow at the South Pole and the Greenland Ice Sheet Project II ice core. *Global Biogeochemical Cycles*, *16*(4), 1129. <https://doi.org/10.1029/2002gb001911>
- Spahni, R., Chappellaz, J., Stocker, T. F., Loulergue, L., Hausammann, G., Kawamura, K., et al. (2005). Atmospheric methane and nitrous oxide of the late Pleistocene from Antarctic ice cores. *Science*, *310*(5752), 1317–1321. <https://doi.org/10.1126/science.1120132>
- Stein, L. Y., & Yung, Y. L. (2003). Production, isotopic composition, and atmospheric fate of biologically produced nitrous oxide. *Annual Review of Earth and Planetary Sciences*, *31*(1), 329–356. <https://doi.org/10.1146/annurev.earth.31.110502.080901>
- Stocker, T. F., & Johnsen, S. J. (2003). A minimum thermodynamic model for the bipolar seesaw. *Paleoceanography*, *18*(4), 1087. <https://doi.org/10.1029/2003pa000920>
- Sutka, R. L., Ostrom, N. E., Breznak, J. A., Gandhi, H., Pitt, A. J., & Li, F. (2006). Distinguishing nitrous oxide production from nitrification and denitrification on the basis of isotopomer abundances. *Applied and Environmental Microbiology*, *72*(1), 638–644. <https://doi.org/10.1128/aem.72.1.638-644.2006>
- Sutka, R. L., Ostrom, N. E., Ostrom, P. H., Gandhi, H., & Breznak, J. A. (2003). Nitrogen isotopomer site preference of N<sub>2</sub>O produced by *Nitrosomonas europaea* and *Methylococcus capsulatus* Bath. *Rapid Communications in Mass Spectrometry*, *17*(7), 738–745. <https://doi.org/10.1002/rcm.968>
- Tans, P. P. (1997). A note on isotopic ratios and the global atmospheric methane budget. *Global Biogeochemical Cycles*, *11*(1), 77–81. <https://doi.org/10.1029/96gb03940>
- Tarasov, L., & Peltier, W. R. (2005). Arctic freshwater forcing of the Younger Dryas cold reversal. *Nature*, *435*(7042), 662–665. <https://doi.org/10.1038/nature03617>
- Tian, H. Q., Xu, R. T., Canadell, J. G., Thompson, R. L., Winiwarter, W., Suntharalingam, P., et al. (2020). A comprehensive quantification of global nitrous oxide sources and sinks. *Nature*, *586*(7828), 248–256. <https://doi.org/10.1038/s41586-020-2780-0>
- Toyoda, S., Kuroki, N., Yoshida, N., Ishijima, K., Tohjima, Y., & Machida, T. (2013). Decadal time series of tropospheric abundance of N<sub>2</sub>O isotopomers and isotopologues in the Northern Hemisphere obtained by the long-term observation at Hateruma Island, Japan. *Journal of Geophysical Research-Atmospheres*, *118*(8), 3369–3381. <https://doi.org/10.1002/jgrd.50221>
- Toyoda, S., Yoshida, N., & Koba, K. (2017). Isotopocule analysis of biologically produced nitrous oxide in various environments. *Mass Spectrometry Reviews*, *36*(2), 135–160. <https://doi.org/10.1002/mas.21459>
- Toyoda, S., Yoshida, N., Urabe, T., Aoki, S., Nakazawa, T., Sugawara, S., & Honda, H. (2001). Fractionation of N<sub>2</sub>O isotopomers in the stratosphere. *Journal of Geophysical Research*, *106*(D7), 7515–7522. <https://doi.org/10.1029/2000jd900680>
- Vilain, G., Garnier, J., Decuq, C., & Lugnot, M. (2014). Nitrous oxide production from soil experiments: Denitrification prevails over nitrification. *Nutrient Cycling in Agroecosystems*, *98*(2), 169–186. <https://doi.org/10.1007/s10705-014-9604-2>
- Wang, Y. J., Cheng, H., Edwards, R. L., An, Z. S., Wu, J. Y., Shen, C. C., & Dorale, J. A. (2001). A high-resolution absolute-dated Late Pleistocene monsoon record from Hulu Cave, China. *Science*, *294*(5550), 2345–2348. <https://doi.org/10.1126/science.1064618>
- Well, R., Eschenbach, W., Flessa, H., von der Heide, C., & Weymann, D. (2012). Are dual isotope and isotopomer ratios of N<sub>2</sub>O useful indicators for N<sub>2</sub>O turnover during denitrification in nitrate-contaminated aquifers? *Geochimica et Cosmochimica Acta*, *90*, 265–282. <https://doi.org/10.1016/j.gca.2012.04.045>
- Well, R., Flessa, H., Jaradat, F., Toyoda, S., & Yoshida, N. (2005). Measurement of isotopomer signatures of N<sub>2</sub>O in groundwater. *Journal of Geophysical Research*, *110*(G2), G02006. <https://doi.org/10.1029/2005jg000044>
- Xu, R., Prentice, I. C., Spahni, R., & Niu, H. S. (2012). Modelling terrestrial nitrous oxide emissions and implications for climate feedback. *New Phytologist*, *196*(2), 472–488. <https://doi.org/10.1111/j.1469-8137.2012.04269.x>
- Yamagishi, H., Westley, M. B., Popp, B. N., Toyoda, S., Yoshida, N., Watanabe, S., et al. (2007). Role of nitrification and denitrification on the nitrous oxide cycle in the eastern tropical North Pacific and Gulf of California. *Journal of Geophysical Research*, *112*(G2), G02015. <https://doi.org/10.1029/2006jg000227>
- Yu, L. F., Harris, E., Lewicka-Szczepak, D., Barthel, M., Blomberg, M. R. A., Harris, S. J., et al. (2020). What can we learn from N<sub>2</sub>O isotope data? - analytics, processes and modelling. *Rapid Communications in Mass Spectrometry*, *34*(20), e8858. <https://doi.org/10.1002/rcm.8858>
- Yung, Y. L., & Miller, C. E. (1997). Isotopic fractionation of stratospheric nitrous oxide. *Science*, *278*(5344), 1778–1780. <https://doi.org/10.1126/science.278.5344.1778>

## References From the Supporting Information

- Friedman, L., & Bigeleisen, J. (1950). Oxygen and nitrogen isotope effects in the decomposition of ammonium nitrate. *Journal of Chemical Physics*, *18*(10), 1325–1331. <https://doi.org/10.1063/1.1747471>
- Jung, M. Y., Well, R., Min, D., Gieseemann, A., Park, S. J., Kim, J. G., et al. (2014). Isotopic signatures of N<sub>2</sub>O produced by ammonia-oxidizing archaea from soils. *The ISME Journal*, *8*(5), 1115–1125. <https://doi.org/10.1038/ismej.2013.205>
- Kaiser, J., Engel, A., Borchers, R., & Röckmann, T. (2006). Probing stratospheric transport and chemistry with new balloon and aircraft observations of the meridional and vertical NO<sub>2</sub> isotope distribution. *Atmospheric Chemistry and Physics*, *6*(11), 3535–3556. <https://doi.org/10.5194/acp-6-3535-2006>
- Keeling, C. D. (1958). The concentration and isotopic abundances of atmospheric carbon dioxide in rural areas. *Geochimica et Cosmochimica Acta*, *13*(4), 322–334. [https://doi.org/10.1016/0016-7037\(58\)90033-4](https://doi.org/10.1016/0016-7037(58)90033-4)
- Maeda, K., Spor, A., Edel-Hermann, V., Heraud, C., Breuil, M. C., Bizouard, F., et al. (2015). NO<sub>2</sub> production, a widespread trait in fungi. *Scientific Reports*, *5*(1), 9697. <https://doi.org/10.1038/srep09697>
- Rohe, L., Anderson, T. H., Braker, G., Flessa, H., Gieseemann, A., Lewicka-Szczepak, D., et al. (2014). Dual isotope and isotopomer signatures of nitrous oxide from fungal denitrification - A pure culture study. *Rapid Communications in Mass Spectrometry*, *28*(17), 1893–1903. <https://doi.org/10.1002/rcm.6975>
- Rolfe, T. C., & Rice, A. L. (2019). Trends in N<sub>2</sub>O and SF<sub>6</sub> mole fractions in archived air samples from Cape Mearns, Oregon (USA), 1978–1996. *Atmospheric Chemistry and Physics*, *19*(13), 8967–8977. <https://doi.org/10.5194/acp-19-8967-2019>
- Santoro, A. E., Buchwald, C., McIlvin, M. R., & Casciotti, K. L. (2011). Isotopic signature of N<sub>2</sub>O produced by marine ammonia-oxidizing archaea. *Science*, *333*(6047), 1282–1285. <https://doi.org/10.1126/science.1208239>
- Schmidt, H. L., Werner, R. A., Yoshida, N., & Well, R. (2004). Is the isotopic composition of nitrous oxide an indicator for its origin from nitrification or denitrification? A theoretical approach from referred data and microbiological and enzyme kinetic aspects. *Rapid Communications in Mass Spectrometry*, *18*(18), 2036–2040. <https://doi.org/10.1002/rcm.1586>

- Sutka, R. L., Adams, G. C., Ostrom, N. E., & Ostrom, P. H. (2008). Isotopologue fractionation during NO<sub>2</sub> production by fungal denitrification. *Rapid Communications in Mass Spectrometry*, 22(24), 3989–3996. <https://doi.org/10.1002/rcm.3820>
- Toyoda, S., Mutoke, H., Yamagishi, H., Yoshida, N., & Tanji, Y. (2005). Fractionation of N<sub>2</sub>O isotopomers during production by denitrifier. *Soil Biology and Biochemistry*, 37(8), 1535–1545. <https://doi.org/10.1016/j.soilbio.2005.01.009>
- Toyoda, S., & Yoshida, N. (1999). Determination of nitrogen isotopomers of nitrous oxide on a modified isotope ratio mass spectrometer. *Analytical Chemistry*, 71(20), 4711–4718. <https://doi.org/10.1021/ac9904563>
- Yamazaki, T., Hozuki, T., Arai, K., Toyoda, S., Koba, K., Fujiwara, T., & Yoshida, N. (2014). Isotopomeric characterization of nitrous oxide produced by reaction of enzymes extracted from nitrifying and denitrifying bacteria. *Biogeosciences*, 11(10), 2679–2689. <https://doi.org/10.5194/bg-11-2679-2014>